

Labor and Welfare; grants from the Ministry of Education, Culture, Sports, Science, and Technology of Japan; a Center-of-Excellence (COE) grant; a Grant-in-Aid for Scientific Research on Innovated Areas "Foundations of Synapse and Neurocircuit Pathology"; and the Core Research for Evolutional Science and Technology (CREST) program of the Japan Science and Technology Agency (JST).

AUTHOR CONTRIBUTIONS

Project planning was done by Y.M., H.A., M.K., F.T., S. Muramatsu and G.S.; experimental work was done by Y.M., H.A., M.K., M.M., Y.-M.J., Z.H., H.D., S. Matsumoto, N.K., M.I., G.T. and S. Muramatsu; data analysis was done by Y.M., H.A., M.K., F.T., S. Muramatsu and G.S.; the manuscript was written by Y.M., H.A., M.K., F.T., S. Muramatsu and G.S.

COMPETING FINANCIAL INTERESTS

The authors declare no competing financial interests.

Published online at <http://www.nature.com/doi/10.1038/nm.2791>.

Reprints and permissions information is available online at <http://www.nature.com/reprints/index.html>.

- La Spada, A.R., Wilson, E.M., Lubahn, D.B., Harding, A.E. & Fischbeck, K.H. Androgen receptor gene mutations in X-linked spinal and bulbar muscular atrophy. *Nature* **352**, 77–79 (1991).
- Kennedy, W.R., Alter, M. & Sung, J.H. Progressive proximal spinal and bulbar muscular atrophy of late onset: a sex-linked recessive trait. *Neurology* **50**, 583–593 (1998).
- Sobue, G. *et al.* X-linked recessive bulbospinal neuronopathy. A clinicopathological study. *Brain* **112**, 209–232 (1989).
- Kim, V.N., Han, J. & Siomi, M.C. Biogenesis of small RNAs in animals. *Nat. Rev. Mol. Cell Biol.* **10**, 126–139 (2009).
- Kim, J. *et al.* A MicroRNA feedback circuit in midbrain dopamine neurons. *Science* **317**, 1220–1224 (2007).
- Karres, J.S., Hilgers, V., Carrera, I., Treisman, J. & Cohen, S.M. The conserved microRNA miR-8 tunes atrophin levels to prevent neurodegeneration in *Drosophila*. *Cell* **131**, 136–145 (2007).
- Lee, Y. *et al.* miR-19, miR-101 and miR-130 co-regulate ATXN1 levels to potentially modulate SCA1 pathogenesis. *Nat. Neurosci.* **11**, 1137–1139 (2008).
- Williams, A.H. *et al.* MicroRNA-206 delays ALS progression and promotes regeneration of neuromuscular synapses in mice. *Science* **326**, 1549–1554 (2009).
- Roshan, R., Ghosh, T., Scaria, V. & Pillai, B. MicroRNAs: novel therapeutic targets in neurodegenerative diseases. *Drug Discov. Today* **14**, 1123–1129 (2009).
- Boudreau, R.L., Rodríguez-Lebrón, E. & Davidson, B.L. RNAi medicine for the brain: progresses and challenges. *Hum. Mol. Genet.* **20**, R21–R27 (2011).
- Katsuno, M. *et al.* Testosterone reduction prevents phenotypic expression in a transgenic mouse model of spinal and bulbar muscular atrophy. *Neuron* **35**, 843–854 (2002).
- Katsuno, M. *et al.* Leuprorelin rescues polyglutamine-dependent phenotypes in a transgenic mouse model of spinal and bulbar muscular atrophy. *Nat. Med.* **9**, 768–773 (2003).
- Adachi, H. *et al.* Heat shock protein 70 chaperone overexpression ameliorates phenotypes of the spinal and bulbar muscular atrophy transgenic mouse model by reducing nuclear-localized mutant androgen receptor protein. *J. Neurosci.* **23**, 2203–2211 (2003).
- Waza, M. *et al.* 17-AAG, an Hsp90 inhibitor, ameliorates polyglutamine-mediated motor neuron degeneration. *Nat. Med.* **11**, 1088–1095 (2005).
- Tokui, K. *et al.* 17-DMAG ameliorates polyglutamine-mediated motor neuron degeneration through well-preserved proteasome function in an SBMA model mouse. *Hum. Mol. Genet.* **18**, 898–910 (2009).
- Eacker, S.M., Dawson, T.M. & Dawson, V.L. Understanding microRNAs in neurodegeneration. *Nat. Rev. Neurosci.* **10**, 837–841 (2009).
- Bilen, J., Liu, N., Burnett, B.G., Pittman, R.N. & Bonini, N.M. MicroRNA pathways modulate polyglutamine-induced neurodegeneration. *Mol. Cell* **24**, 157–163 (2006).
- Schaefer, A. *et al.* Cerebellar neurodegeneration in the absence of microRNAs. *J. Exp. Med.* **204**, 1553–1558 (2007).
- Kaspar, B.K. *et al.* Retrograde viral delivery of IGF-1 prolongs survival in a mouse ALS model. *Science* **301**, 839–842 (2003).
- Towne, C. *et al.* Efficient transduction of non-human primate motor neurons after intramuscular delivery of recombinant AAV serotype 6. *Gene Ther.* **17**, 141–146 (2010).
- Dominguez, E. *et al.* Intravenous scAAV9 delivery of a codon-optimized SMN1 sequence rescues SMA mice. *Hum. Mol. Genet.* **20**, 681–693 (2011).
- Fu, H., Dirosario, J., Killedar, S., Zaraspe, K. & McCarty, D.M. Correction of neurological disease of mucopolysaccharidosis IIIB in adult mice by rAAV9 trans-blood-brain barrier gene delivery. *Mol. Ther.* **19**, 1025–1033 (2011).
- Petrs-Silva, H. *et al.* Novel properties of tyrosine-mutant AAV2 vectors in the mouse retina. *Mol. Ther.* **19**, 293–301 (2011).
- Hui, A.B. *et al.* Robust global micro-RNA profiling with formalin-fixed paraffin-embedded breast cancer tissues. *Lab. Invest.* **89**, 597–606 (2009).
- Maru, D.M. MicroRNA-196a is a potential marker of progression during Barrett's metaplasia-dysplasia-invasive adenocarcinoma sequence in esophagus. *Am. J. Pathol.* **174**, 1940–1948 (2009).
- Yekta, S., Shih, I.H. & Bartel, D.P. MicroRNA-directed cleavage of HOXB8 mRNA. *Science* **304**, 594–596 (2004).
- Hornstein, E. *et al.* The microRNA miR-196 acts upstream of Hoxb8 and Shh in limb development. *Nature* **438**, 671–674 (2005).
- Pedersen, I.M. *et al.* Interferon modulation of cellular microRNAs as an antiviral mechanism. *Nature* **449**, 919–922 (2007).
- Dhaenens, C.M. *et al.* Mis-splicing of *Tau* exon 10 in myotonic dystrophy type 1 is reproduced by overexpression of CELF2 but not by MBNL1 silencing. *Biochim. Biophys. Acta* **1812**, 732–742 (2011).
- Natarajan, G. *et al.* CUGBP2 downregulation by prostaglandin E2 protects colon cancer cells from radiation-induced mitotic catastrophe. *Am. J. Physiol. Gastrointest. Liver Physiol.* **294**, G1235–G1244 (2008).
- Subramaniam, D. *et al.* RNA binding protein CUGBP2/CELF2 mediates curcumin-induced mitotic catastrophe of pancreatic cancer cells. *PLoS ONE* **6**, e16958 (2011).



ONLINE METHODS

Construction of DNA plasmids. We constructed cDNA expression plasmids encoding full-length AR by subcloning AR cDNA derived from pSP64-AR24 and pSP64-AR97 (ref. 32) into the pCR3.1 mammalian expression vector (Life Technologies). We carried out an L55 L56 L57 (CTGCTGCTG) deletion of AR-24Q and AR-97Q as follows: the pBS+AflII plasmid was generated by the insertion of an AflII linker into the EcoRV site of pBluescript II KS(-). We excised the 417-bp fragment of 24Q and the 636-bp fragment of 97Q from pCR3.1-AR-24Q and -97Q using SmaI and AflII and cloned it into the SmaI and AflII sites of pBS+AflII to create pBS-24Q and -97Q. pBS- Δ CUG-24Q and -97Q were constructed by inserting the double-stranded oligomer CCAGTTTGCA into pBS-24Q and -97Q digested with NarI-PstI (blunted). Finally, we re-excised the pBS- Δ CUG-24Q and -97Q with SmaI-AflII and inserted this fragment between the SmaI and AflII sites of pCR3.1-AR to form pCR3.1-AR Δ CUG-24Q and -97Q.

The CAG repeat deletion of the AR construct was generated using a KOD-Plus-Mutagenesis kit (Toyobo) with the forward primer 5'-CAAGAG ACTAGCCCCAGGCAGCAGC-3' and the reverse primer 5'-CAGCAGCA GCAAACCTGGCGCCG-3'. The DNA plasmid expressing human CELF2 was kindly provided by T. Cooper (Professor, Department of Pathology and Immunology, Baylor College of Medicine). The siRNA-resistant construct was generated by changing the siRNA targeted sequence (5'-GAATGCACTGCACA ATATT-3') of pcDNA3.1/HisC-CELF2 to 5'-AAACGCGCTACATAACATC-3' (mutated nucleotides are underlined) using a KOD-Plus-Mutagenesis kit (Toyobo) with the forward primer 5'-ACATAACATCAAACTTTACCTGG GATGCATCATCCCA-3' and the reverse primer 5'-AGCGCGTTTTGGGCC TCAAGTGCAGCTTTTCTTGATA-3'. The sequences of all mutations and the CAG repeat length were confirmed using a CEQ 8000 Genetic Analysis System (Beckman Coulter). We used the original pcDNA3.1/HisC vector lacking the insertions in the multiple cloning sites as a mock vector.

Co-transfection of DNA plasmids with either synthetic miRNA or siRNA into cultured cells. The sequences of the siRNA target for CELF2 mRNA are 5'-GAATGCACTGCACAATATT-3' (accession number NM_001025076), 5'-CACCTATCGTGGTGAAGTT-3' (accession number NM_001025076) and 5'-CACAGTATCTGGCGCTCCT-3' (accession number NM_001025076). All of the siRNAs were purchased from Sigma-Aldrich. A scrambled control siRNA (MISSION siRNA Universal Negative Control SIC-001; Sigma-Aldrich), synthetic miR-196a (MISSION microRNA Mimics -hsa-miR-196a; Sigma-Aldrich), synthetic miR-196b (MISSION microRNA Mimics -hsa-miR-196b; Sigma-Aldrich), synthetic miR-496 (MISSION microRNA Mimics -hsa-miR-496; Sigma-Aldrich), synthetic miR-323-3p (MISSION microRNA Mimics -hsa-miR-323-3p; Sigma-Aldrich), synthetic miR-29b* (Syn-mmu-miR-29b-1* miScript miRNA Mimic; Qiagen), anti-miR-196a antisense (anti-hsa-miR-196a miScript miRNA Inhibitor; Qiagen) and negative control miRNA (MISSION microRNA Mimic, Human, Negative Control 1; Sigma-Aldrich) were purchased. We plated HEK293T cells onto six-well dishes and co-transfected each dish with 0.5 μ g of the vector containing the following: AR-24Q, AR-97Q, Δ CUG-AR-24Q, Δ CUG-AR-97Q or AR-0Q; 2.0 μ g of the vector containing CELF2, siRNA-resistant CELF2 or mock; and either 25 nM synthetic miRNA or 25 nM siRNA molecules. We used Lipofectamine 2000 (Life Technologies) as a transfection reagent in the cases in which all of the RNAi molecules purchased from Sigma-Aldrich were transfected into the HEK293T cells or Neuro2a cells. For the transfection of synthetic miR-29b* (Syn-mmu-miR-29b-1* miScript miRNA Mimic; Qiagen) and anti-miR-196a antisense (anti-hsa-miR-196a miScript miRNA Inhibitor; Qiagen) into HEK293T cells, we used the Attractene Transfection Reagent (Qiagen) as a transfection reagent. Neither the scrambled control siRNA nor the negative control miRNA matched any human or mouse mRNA. For the transfection of all of the RNAi molecules purchased from Sigma-Aldrich into human fibroblasts, we used jetPRIME (Polyplus-transfection SA) as a transfection reagent with a high amount of RNAi molecules because the human fibroblasts exhibited a lower transduction efficiency of RNAi molecules compared with those of the HEK293T cells and Neuro2a cells, for which we used Lipofectamine 2000 (Life Technologies) as a transfection reagent. The transfected cells were cultured for 48 h before being processed for western blotting and RNA analysis.

Protein expression analysis. We did western blotting and densitometric analyses as previously described^{12,14}. We used the following primary antibodies: AR-specific antibody (1:5,000, N20 or 1:5,000, H280; Santa Cruz), CELF2-specific antibody (1:5,000, ab50734; Abcam), α -tubulin-specific antibody (1:5,000, T9026; Sigma-Aldrich), GFP-specific antibody (1:5,000, M048-3; MBL), GFAP-specific antibody (1:2,000, 814369; Boehringer Mannheim Biochemicals), IGF-1-specific antibody (1:1,000, ab9572; Abcam) and cleaved caspase-3-specific antibody (1:2,000, 9661; Cell Signaling Technology).

Quantitative real-time PCR. For cultured cells, the total RNA was extracted from HEK293T cells using the QIAzol Lysis Reagent (Qiagen) and reverse transcribed using Superscript VILO (Life Technologies). The complementary DNAs were then used for real time PCR using the SsoFast EvaGreen Supermix (Bio-Rad Laboratories). For mouse tissue analysis, the total RNA was isolated from the thoracic spinal cord and skeletal muscles of mice using the QIAzol Lysis Reagent (Qiagen) and reverse transcribed with the miScript Reverse-Transcription Kit (Qiagen). The complementary DNAs were then used for real time PCR using the SYBR Green Supermix (Qiagen). We did the amplification, detection and data analysis using a Bio-Rad iCycler system (Bio-Rad Laboratories). The crossing threshold values for the mRNAs of the individual genes were normalized to β -2-microglobulin (B2MG). The crossing threshold values for the miRNA of the individual genes were normalized to the U6 small nuclear RNA 2. Changes in the expression of mRNA and miRNA were expressed as a fold change relative to the control.

We used the following primers in this study. The sequences of the hsa-AR primers were: forward, 5'-GGCTATGAATGTCAGCCCAT-3'; reverse, 5'-TTGAGG CTAGAGAGCAAGGC-3'. These hsa-AR primers discriminated between the human AR mRNA and the mouse AR mRNA. The sequences of the mmu-AR primers were: forward, 5'-TGGGACCTTGATGGAGA ACTA-3'; reverse, 5'-ACAGATCAGGCAGGTCTTCTGG-3'. These mmu-AR primers discriminated between the mouse AR mRNA and the human AR mRNA. The sequences of the hsa-CELF2 primers were: forward, 5'-CTGGCGGAAACAACACTCTG-3'; reverse, 5'-TCTAAGCCCTTGGCCTCCTC-3'. The sequences of the mmu-CELF2 primers were: forward, 5'-GCTGTGCGTTTGTACATTTTC-3'; reverse, 5'-TGTCAGC AAACCTCACCACGAT-3'. The sequences of the hsa-B2MG primers were: forward, 5'-CTGAAGCTGACAGCATTCGG-3'; reverse, 5'-GTCAACTCAATGT CGGATGGATG-3'. The sequences of the mmu-B2MG primers were: forward, 5'-AAGCCGAACATACTGAACTGC-3'; reverse, 5'-GTGTGAGCCAGGATATA GAAAGAC-3'. The sequences of the hsa-IGF-1 primers were: forward, 5'-GCTGT GATCTAAGGAGGCTGGA-3'; reverse, 5'-TTCCTGCACTCCCTCTACTTGCA TGGATG-3'. The primers used for the detection of miR-196a, miR-196b and U6 small nuclear RNA 2 were the Hs_miR-196a_1 miScript Primer Assay (Qiagen), the Hs_miR-196b_2 miScript Primer Assay (Qiagen) and the Hs_RNU6-2_1 miScript Primer Assay (Qiagen), respectively.

Immunoprecipitation-coupled qRT-PCR. We did coimmunoprecipitation using an affinity-purified CELF2 antibody (15 μ g per sample, ab50734; Abcam) followed by RNA isolation using the RiboCluster Profiler RIP-Assay kit (MBL International Corporation) according to the manufacturer's suggested protocols. Rabbit immunoglobulin G, supplied by the manufacturer, was used as a control, and the immunoprecipitated RNA was converted to cDNA using Superscript VILO (Life Technologies) and analyzed by qRT-PCR for the differential expression of AR mRNA using the following primers: forward, 5'-GGCTATGAATGTCAGCCCAT-3'; reverse, 5'-TTGAGGCT AGAGAGCAAGGC-3'.

RNA stability assay. We added actinomycin D (10 mg ml⁻¹ final concentration), a potent inhibitor of mRNA synthesis, to the HEK293T cells at 24 h after co-transfection of DNA plasmid and RNAi molecules. The total RNA was extracted from the cells at 0–4 h after treatment, and the RNA was then subjected to qRT-PCR as described above. The data are presented as values relative to the levels of expression detected in the transfected cells harvested at the time of actinomycin D treatment.

miRNA microarray analysis. The total RNA was extracted from the thoracic spinal cord of transgenic SBMA mice (AR-97Q) and wild-type mice (AR-24Q)





at 15 weeks of age and used for the miRNA microarray analysis conducted by TaKaRa Bio. Each group consisted of two mice.

miRNA *in situ* hybridization. To investigate the cell-specific distribution of miRNA in mouse spinal tissues, we did *in situ* hybridization using 5'- and 3'-end digoxigenin (DIG)-labeled locked nucleic acid (LNA)-modified DNA oligonucleotides complementary to the mature miRNA (Exiqon). In this study, we examined the global expression of miR-196a in mouse tissue sections that had been prepared as previously described^{13–15,33}. The LNA-miR-196a and LNA-scrambled oligonucleotides (negative control) were used in this analysis.

We did the *in situ* hybridization of mouse tissue sections using a Ventana Discovery system (Ventana Medical Systems). Briefly, 5'- and 3'-end DIG-labeled LNA probes were stained with digoxigenin-AP-specific Fab fragments (1:800, 1093274; Roche). The sections were then counterstained using Red Counterstain II (780-2218; Ventana), and the signals were visualized under a standard light microscope.

Development of the AAV vector with simultaneous expression of miRNA and EGFP. The AAV vector plasmids contained an expression cassette consisting of a human cytomegalovirus immediate-early promoter, followed by cDNA encoding EGFP, miR-196a or the miR-mock sequence, and a woodchuck hepatitis virus post-transcriptional regulatory element between the inverted terminal repeats of the AAV3 genome. We synthesized the AAV9 *vp* cDNA, and this sequence was identical to that previously described³⁴ except for the substitution of adenine with thymidine at position 1337, which introduced an amino acid change from tyrosine to phenylalanine at position 446 (ref. 23). The recombinant AAV vectors were produced by transient transfection of HEK293 cells using the vector plasmid, an AAV3 *rep* and AAV9 *vp* expression plasmid and an adenoviral helper plasmid, pHelper (Stratagene), as previously described³⁵. We purified the recombinant viruses by isolation from two sequential continuous CsCl gradients, and then the viral titers were determined by qRT-PCR. The cDNA sequences of miR-196a and miR-mock are as follows. miR-196a: 5'-TGAGCCGGGACTGTTGAGTGAAGTAGGTAGTTTCATGTTGTTGGGCTGGCTTTCTGAACACAACGCATCAAA CCACCTGATTTCATGGCAGTTACTGCTTC-3'. miR-mock: 5'-GTATTGCGTCTGTACACTCACCGTTTGGCCACTGACTGACGGTGAGTGCAG ACGCAATA-3'.

The neurological and behavioral assessment of the SBMA model mice. We generated and maintained the AR-24Q and AR-97Q mice as previously described¹². All of the animal experiments were carried out in accordance with the National Institutes of Health Guide for the Care and Use of Laboratory Animals and were approved by the Nagoya University Animal Experiment Committee. We did the mouse rotarod task and cage activity assessment as described previously^{12,14}. The investigators who carried out the behavioral assessments were blinded to the treatment conditions.

Immunohistochemistry, immunofluorescence, histochemistry and histopathology. The preparation of the tissue sections, immunohistochemistry, immunofluorescence and histopathology were done as previously described^{11–15,33}.

To quantify the 1C2-positive cells, we counted the 1C2-positive cells within the thoracic spinal cord and quadriceps femoris muscle for each individual mouse as previously described^{12,14}. For choline acetyltransferase immunolabeling, the sections were first microwaved for 20 min in 50 mM citrate buffer, pH 6.0. For polyglutamine (1C2 antibody) immunolabeling, the sections were treated with formic acid for 5 min at room temperature. We treated all of the specimens with TNB blocking buffer (PerkinElmer) before incubation with primary antibodies. The immunohistochemical sections were then imaged using an optical microscope (BX51, Olympus), and the immunofluorescent specimens were photographed using an upright microscope (LSM710, Zeiss). We used the following primary antibodies: choline acetyltransferase-specific antibody (1:100, AB144; Millipore), mouse GFP-specific antibody (1:200, M048-3;

MBL), mouse expanded polyQ antibody (1:10,000, 1C2; Millipore) and mouse GFAP-specific antibody (1:1,000, 814369; Boehringer Mannheim Biochemica). The primary antibodies were probed with biotinylated anti-species-specific IgG secondary antibodies (Vector Laboratories), and the immune complexes were visualized using streptavidin-horseradish peroxidase (Dako) and 3,3'-diaminobenzidine as a substrate. We used Alexa-conjugated secondary antibodies (Life Technologies) for immunofluorescence. We assessed the size of the motor neuron in the thoracic spinal cord of the SBMA mice treated with AAV-miR-196a or AAV-miR-mock as previously described³³. The stained sections were then examined and imaged using a BIOREVO BZ-9000 system (Keyence). To assess the GFAP expression levels in the thoracic spinal anterior horn cells, we quantified the immunohistochemistry signal intensities in at least ten transverse sections obtained from each mouse. The images of individual anterior horn on transverse sections of thoracic spinal cord with signals for GFAP were captured at the desired magnification and stored using image software (Keyence). The levels of GFAP staining in the images were quantitatively analyzed using image analysis software (Dynamic cell count BZ-HIC software, Keyence). The signal intensities were expressed as individual intracellular areas of GFAP staining (μm^2) in the unilateral thoracic spinal anterior horn.

Assay of serum testosterone levels in SBMA mice. We sacrificed SBMA mice treated with AAV-miR-196a or AAV-miR-mock at 12 weeks of age, collected 1 ml of blood by cardiocentesis and conducted an assay for serum testosterone levels using a radioimmunoassay (Mitsubishi Kagaku Bio-Clinical Laboratories).

The fibroblasts and thoracic spinal cords of patients. We obtained biopsy specimens of fibroblasts of scrotal skin from three patients genetically diagnosed with SBMA and three disease control subjects. The CAG repeat lengths of the patients with SBMA were 48, 50 and 52. The disease control subjects included three male individuals who were diagnosed with a cerebrovascular disease.

We obtained autopsy specimens of the thoracic spinal cord from three patients genetically diagnosed with SBMA (52-, 66- and 78-year-old males) and from disease control subjects (58-, 61- and 75-year-old males). The CAG repeat lengths of three patients with SBMA were 48, 49 and 50, respectively. The disease control subjects included individuals diagnosed with Parkinson's disease ($n = 2$) and dementia with Lewy body disease ($n = 1$). The collection of human tissues and their use for this study were approved by the Ethics Committee of Nagoya University Graduate School of Medicine. We obtained informed consent from the patients.

The pulse-chase labeling assay. HEK293T cells were transfected as previously described, starved for 1 h and then labeled for an additional 1 h with 150 mCi ml^{-1} of EXPRE³⁵S³⁵S Protein Labeling Mix [³⁵S] (PerkinElmer Life & Analytical Sciences). We chased the HEK293T cells for the indicated time intervals. We then did immunoprecipitation using equivalent amounts of protein lysates as previously described¹⁴ and analyzed the expression levels using phosphorimaging (Typhoon 8600 phosphorimager; Amersham) and Image Gauge software, version 4.22 (Fujifilm).

The apoptosis assay. We plated Neuro2a neuronal lineage cells onto six-well dishes and co-transfected each dish with 25 nM synthetic miR-196a using Lipofectamine 2000 (Life Technologies) according to the manufacturer's instructions. After 24 h, we treated the Neuro2a cells with 1 μM staurosporine, a major inducer of apoptosis, for 6 h. Next, we processed and probed the western blots with a cleaved caspase-3 antibody. The effect of miR-196a on apoptosis in the Neuro2a cells was then assessed by the change in the relative expression levels of cleaved caspase-3 protein.

Statistical analyses. We analyzed the results by unpaired *t* tests, Dunnett tests and two-way ANOVA followed by Bonferroni tests for individual paired comparison using IBM SPSS statistics version 19 for Windows (IBM). We used log-rank tests for the assessment of the survival rate in Fig. 3d using IBM

SPSS statistics version 19 for Windows (IBM). *P* values of less than 0.05 were considered statistically significant.

32. Kobayashi, Y. *et al.* Chaperones Hsp70 and Hsp40 suppress aggregate formation and apoptosis in cultured neuronal cells expressing truncated androgen receptor protein with expanded polyglutamine tract. *J. Biol. Chem.* **275**, 8772–8778 (2000).

33. Katsuno, M. *et al.* Disrupted transforming growth factor- β signaling in spinal and bulbar muscular atrophy. *J. Neurosci.* **30**, 5702–5712 (2010).

34. Gao, G. *et al.* Clades of adeno-associated viruses are widely disseminated in human tissues. *J. Virol.* **78**, 6381–6388 (2004).

35. Li, X.G. *et al.* Viral-mediated temporally controlled dopamine production in a rat model of Parkinson disease. *Mol. Ther.* **13**, 160–166 (2006).



c-Abl Inhibition Delays Motor Neuron Degeneration in the G93A Mouse, an Animal Model of Amyotrophic Lateral Sclerosis

Ryu Katsumata¹, Shinsuke Ishigaki^{1,2,3}, Masahisa Katsuno¹, Kaori Kawai¹, Jun Sone¹, Zhe Huang¹, Hiroaki Adachi¹, Fumiaki Tanaka¹, Fumihiko Urano^{2,4}, Gen Sobue^{1,3*}

1 Department of Neurology, Nagoya University Graduate School of Medicine, Tsurumai-cho, Showa-ku, Nagoya, Japan, **2** Program in Gene Function and Expression, University of Massachusetts Medical School, Worcester, Massachusetts, United States of America, **3** Core Research for Evolutional Science and Technology, Japan Science and Technology Agency, Saitama, Japan, **4** Program in Molecular Medicine, University of Massachusetts Medical School, Worcester, Massachusetts, United States of America

Abstract

Background: Amyotrophic lateral sclerosis (ALS) is a fatal neurodegenerative disease characterized by progressive death of motor neurons. Although the pathogenesis of ALS remains unclear, several cellular processes are known to be involved, including apoptosis. A previous study revealed the apoptosis-related gene c-Abl to be upregulated in sporadic ALS motor neurons.

Methodology/Findings: We investigated the possibility that c-Abl activation is involved in the progression of ALS and that c-Abl inhibition is potentially a therapeutic strategy for ALS. Using a mouse motor neuron cell line, we found that mutation of Cu/Zn-superoxide dismutase-1 (SOD1), which is one of the causative genes of familial ALS, induced the upregulation of c-Abl and decreased cell viability, and that the c-Abl inhibitor dasatinib inhibited cytotoxicity. Activation of c-Abl with a concomitant increase in activated caspase-3 was observed in the lumbar spine of G93A-SOD1 transgenic mice (G93A mice), a widely used model of ALS. The survival of G93A mice was improved by oral administration of dasatinib, which also decreased c-Abl phosphorylation, inactivated caspase-3, and improved the innervation status of neuromuscular junctions. In addition, c-Abl expression in postmortem spinal cord tissues from sporadic ALS patients was increased by 3-fold compared with non-ALS patients.

Conclusions/Significance: The present results suggest that c-Abl is a potential therapeutic target for ALS and that the c-Abl inhibitor dasatinib has neuroprotective properties *in vitro* and *in vivo*.

Citation: Katsumata R, Ishigaki S, Katsuno M, Kawai K, Sone J, et al. (2012) c-Abl Inhibition Delays Motor Neuron Degeneration in the G93A Mouse, an Animal Model of Amyotrophic Lateral Sclerosis. PLoS ONE 7(9): e46185. doi:10.1371/journal.pone.0046185

Editor: Thomas H. Gillingwater, University of Edinburgh, United Kingdom

Received: March 21, 2012; **Accepted:** August 28, 2012; **Published:** September 25, 2012

Copyright: © 2012 Katsumata et al. This is an open-access article distributed under the terms of the Creative Commons Attribution License, which permits unrestricted use, distribution, and reproduction in any medium, provided the original author and source are credited.

Funding: This work was supported by a Center-of-Excellence (COE) grant from the Ministry of Education, Culture, Sports, Science and Technology of Japan [http://w3serv.nagoya-u.ac.jp/coemed/en/index.html]; a Grant-in-Aid for Scientific Research on Innovative Areas "Foundation of Synapse and Neurocircuit Pathology" [http://www.tmd.ac.jp/mri/shingakujutu/index-e.html], and Grant-in-Aids from Ministry of Education, Culture, Sports, Science, and Technology of Japan [http://www.jps.go.jp/english/e-grants/index.html]; grants from the Ministry of Health, Labor and Welfare of Japan [http://www.mhlw.go.jp/english/policy/other/research-projects/index.html]; and Core Research for Evolutional Science and Technology (CREST) from the Japan Science and Technology Agency (JST) [http://www.sss.jst.go.jp/english/index.html]. The funders had no role in study design, data collection and analysis, decision to publish, or preparation of the manuscript.

Competing Interests: The authors have declared that no competing interests exist.

* E-mail: sobueg@med.nagoya-u.ac.jp

Introduction

Amyotrophic lateral sclerosis (ALS) is a neurodegenerative disease characterized by selective loss of upper and lower motor neurons in the cerebral cortex, brain stem, and spinal cord [1,2]. Many genes have been identified as involved in familial ALS cases, including Cu/Zn-superoxide dismutase-1 (SOD1) [3,4,5]. Approximately 5–10% of ALS cases are familial, and 20% of familial ALS cases are associated with mutations in the SOD1 gene [3]. Several hypotheses for the pathogenesis of ALS have been proposed, including oxidative stress, glutamate excitotoxicity, mitochondrial dysfunction, and neuroinflammation, all of which eventually lead to the death of motor neurons [6,7,8,9]. Many studies using mutant SOD1 transgenic animals have explored the

precise cellular mechanisms of motor neuron death; however, no therapeutic drugs have been developed to date except for riluzole, which has only limited effects. Since most cases of ALS are sporadic, the development of ALS drug therapies based on the pathology of sporadic ALS (sALS) is feasible.

Previously, we performed microarray analyses combined with laser-capture microdissection to investigate the gene expression profiles of spinal motor neurons isolated from autopsied patients with sALS [10]. We found altered expression of many genes, including dynactin 1, early growth response-3, acetyl-CoA transporter, death receptor 5, and cyclin C [10,11]. In that study, a 4.41-fold increase in the amount of c-Abl mRNA was detected in the motor neurons of sALS patients [10]. These findings raised the

possibility that upregulation of c-Abl in motor neurons contributes to motor neuron degeneration and that activation of this pathway may be one of the pathologic features of ALS.

c-Abl is a ubiquitous non-receptor tyrosine kinase that was originally identified as the cellular homolog of the v-abl gene, an oncogene carried by the Abelson murine leukemia virus [12]. Bcr-Abl hybrid protein, which is one of the oncogenic forms of c-Abl fusion kinase, causes chronic myelogenous leukemia (CML) and Philadelphia chromosome-positive adult acute lymphoblastic leukemia (Ph+ALL) [13,14]. The kinase activity of c-Abl is regulated by phosphorylation. Tyrosine 245 (Tyr245) and tyrosine 412 (Tyr412) are well-established regulatory phospho-tyrosine residues that are required for c-Abl activation [15]. In response to various stimuli, c-Abl regulates cytoskeletal rearrangement, cell migration, cell-cell adhesion, cell proliferation, and apoptosis [16,17,18,19,20]. On exposure to stressors, such as DNA damage or oxidative stress, c-Abl has been implicated in cell growth arrest and caused apoptotic cell death in association with p73 [21,22], PKC delta [23], and CDK5 [24,25]. Recently, neural functions of c-Abl have also been described: c-Abl participates in neuronal development and neurite outgrowth [26,27], and has also been implicated in the pathogenesis of Alzheimer's disease [28,29].

In the present study, we investigated c-Abl activation in a mutant SOD1 transgenic ALS mouse model and in ALS patients, and we demonstrated that the c-Abl inhibitor dasatinib has a protective effect on motor neuron degeneration in G93A-SOD1 transgenic ALS mice (G93A mice).

Results

Inducible expression of wild-type and mutant SOD1 in NSC-34 cells

To investigate the expression and activity levels of c-Abl in human mutant SOD1-expressing motor neurons, we established an inducible system of NSC-34 cells able to express either human wild-type or mutant (G93A, G85R) SOD1 protein. Western blot analysis confirmed that myc-tagged human SOD1 proteins were induced by doxycycline in these cell lines (Fig. 1A). Myc-tagged human SOD1 demonstrated lower mobility than mouse endogenous SOD1. NSC-34 cells were well differentiated in low-serum medium with extended neuritic processes, a morphological marker of neuronal cell maturation and differentiation [30]. As a motor neuron-mimicking model, we used NSC-34 cells with serum-free medium to measure cytotoxicity. Cell viability was examined using the MTS-based cell proliferation assay at 48 h after the induction of SOD1 proteins, and we found that both G93A and G85R mutant SOD1s significantly decreased cell viability in comparison with wild-type SOD1 ($P<0.05$ for G93A, $P<0.01$ for G85R) (Fig. 1B). The cytotoxicity of mutant SOD1s was also measured by lactate dehydrogenase (LDH) release assay at 48 h after the induction of SOD1 proteins. The results demonstrated that both G93A and G85R mutant SOD1s significantly increased cytotoxicity in comparison with wild-type SOD1 ($P<0.05$ for G93A, $P<0.01$ for G85R) (Fig. 1C).

c-Abl activation caused by mutant SOD1 in NSC-34 cells

We then investigated whether overexpression of mutant SOD1s influenced the expression of c-Abl. Western blot analysis revealed that the expression of c-Abl was greater in cells expressing mutant SOD1s (G93A and G85R) than cells expressing wild-type SOD1 (Fig. 2A). These differences were much more prominent when phospho-specific antibodies for each of 2 distinct tyrosine residues (Tyr245 and Tyr412) were used for the western blot analysis. Densitometric analysis confirmed that mutant SOD1 significantly

increased the expression and phosphorylation of c-Abl ($P<0.05$) (Fig. 2B). Increased c-Abl mRNA expression in cells overexpressing mutant SOD1s was also confirmed by quantitative RT-PCR (Fig. 2C).

Dasatinib attenuates the cytotoxicity of mutant SOD1s in NSC-34 cells

To examine whether the inhibition of c-Abl kinase influenced the cytotoxicity of mutant SOD1s, we evaluated the effect of dasatinib, a blood-brain barrier (BBB)-permeable c-Abl inhibitor, on c-Abl activity in NSC-34 cells expressing different forms of SOD1. Cells overexpressing SOD1 were treated with increasing concentrations of dasatinib for 24 h and analyzed by western blotting. Dasatinib effectively suppressed the phosphorylation of c-Abl in all cell lines (Fig. 3A). Since dasatinib is a dual c-Abl/c-Src kinase inhibitor [31], in order to clarify the specificity of c-Abl for motor neuronal cytotoxicity, we also performed cell proliferation and cell death assays with SU6656, which preferentially inhibits c-Src compared to c-Abl. SU6656 effectively suppressed the phosphorylation of c-Src in all cell lines (Fig. 3A). Cell viability and cell death assays confirmed that dasatinib significantly reduced the cytotoxicity of mutant SOD1s ($P<0.05$), whereas SU6656 did not (Fig. 3B, C).

Upregulation and activation of c-Abl in G93A mice

To determine whether c-Abl upregulation also occurs in G93A mice, we measured mRNA and protein levels of c-Abl in the lumbar spinal cords of G93A and control mice at age 10 weeks (pre-symptomatic stage), 14 weeks (symptomatic stage), and 18 weeks (terminal stage) by quantitative RT-PCR and western blot analyses. The protein expression of c-Abl in the lumbar spinal cords of G93A mice was increased as early as 10 weeks compared with control littermates (Fig. 4A). A remarkable increase in the phosphorylation of c-Abl was also evident even at the pre-clinical stage of 10 weeks. The increase in c-Abl protein was paralleled by an induction of c-Abl mRNA in the spinal cords of G93A mice (Fig. 4B). Consistent with the western blot analyses and quantitative RT-PCR, immunoreactivity for c-Abl and phosphorylated c-Abl (Tyr245 and Tyr412) was increased in the lumbar spinal neurons of G93A mice compared with those of control littermates (Fig. 4C). We quantified the signal intensity of phosphorylated c-Abl immunofluorescence in motor neurons (Tyr412 and Tyr245) using Image J software. Phosphorylated c-Abl immunoreactivity in G93A mice was significantly increased compared to control mice with both antibodies ($P<0.01$), which indicated that c-Abl was activated at an early stage of disease in this mouse model of ALS (Fig. S1).

The effect of dasatinib on survival and disease progression in G93A mice

Survival of G93A mice was improved by dasatinib at a dose of 25 mg/(kg·day) compared with vehicle treatment ($P<0.01$, 25 mg/(kg·day) vs. vehicle), whereas a lower dose of dasatinib (5 mg/(kg·day)) had no significant effect on life span (Fig. 5). Weight loss was also ameliorated by dasatinib at a dose of 25 mg/(kg·day) compared with vehicle treatment (Fig. 5, 2-way ANOVA, $P<0.01$, 25 mg/(kg·day) vs. vehicle). The administration of dasatinib at 25 mg/(kg·day) similarly alleviated motor dysfunction measured by grip strength (2-way ANOVA, $P<0.01$, 25 mg/(kg·day) vs. vehicle). Dasatinib did not significantly ameliorate the physical function assessed by rotarod, although a beneficial tendency was observed. Dasatinib did not alter the neuromuscular

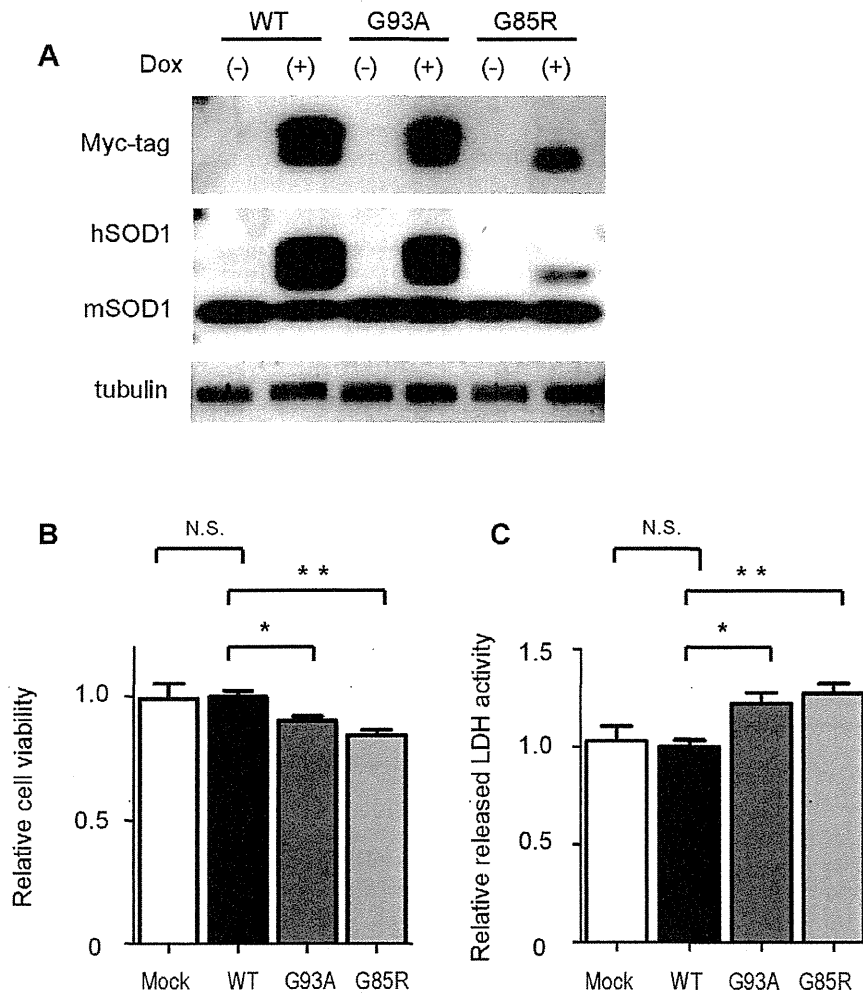


Figure 1. Inducible expression system of wild-type and mutant SOD1s in NSC-34 cells. A: NSC-34 cells were stably transduced with an inducible lentivirus expressing human Myc-tagged wild-type or mutant SOD1 protein. Cells were cultured with or without doxycycline (Dox, 2 μ g/ml) for 48 h to induce SOD1 protein. Tubulin is shown as a loading control. hSOD1 and mSOD1 indicate human SOD1 and mouse endogenous SOD1, respectively. B: Cell viability assay based on the MTS method showed that overexpression of both types of mutant SOD1, G93A and G85R, caused cytotoxicity in serum-free culture medium. Mock indicates mock-transfected NSC-34 cells. Data are presented as mean \pm SEM. Statistics were evaluated using 1-way ANOVA with Dunnett's post-hoc test. * P <0.05, ** P <0.01. C: Cytotoxicity detection assay using the LDH release method revealed that overexpression of both types of mutant SOD1, G93A and G85R, caused cytotoxicity in serum-free culture medium. Data are presented as mean \pm SEM. Statistics were evaluated using 1-way ANOVA with Dunnett's post-hoc test. * P <0.05, ** P <0.01. doi:10.1371/journal.pone.0046185.g001

function or body weight of non-transgenic littermates at any of the doses tested (data not shown).

The effect of dasatinib on motor neuron survival and innervation status of neuromuscular junctions (NMJs) in G93A mice

Paraffin-embedded sections of the lumbar spinal cord (L1-3) from 120-day-old mice were analyzed immunohistochemically using anti-choline acetyltransferase (ChAT) antibody (Fig. 6A). The number of ChAT-positive motor neurons in the lumbar spinal cord was significantly preserved in mice treated with dasatinib at doses of 15 mg/(kg·day) or higher compared with vehicle-treated control mice (P <0.05) (Fig. 6B). To evaluate changes in the size of ChAT-positive motor neurons, we quantified the cell body areas of ChAT-positive motor neurons using Image J

software. The size of motor neurons in dasatinib-treated mice was significantly preserved compared to vehicle-treated controls (P <0.05) (Fig. 6C). To investigate the innervation status of neuromuscular junctions (NMJs), frozen quadriceps femoris specimens were collected from 120-day-old mice and stained with alpha-bungarotoxin (BuTX) (red) and anti-synaptophysin (green) or anti-SMI31 (green) antibodies (Fig. 6D). We observed BuTX-positive NMJs (treated and control groups; n = 3 mice per group, 100 NMJs per mouse) using confocal laser scanning microscopy and counted double- (red and green) or single- (red)-immunostained NMJs. Figure 6E summarizes the ratio of double-immunostained (innervated) NMJs to total NMJs. Dasatinib significantly ameliorated the destruction of NMJ innervation in G93A mice at doses of 5, 15, and 25 mg/(kg·day) compared to vehicle treatment (P <0.05) (Fig. 6E).

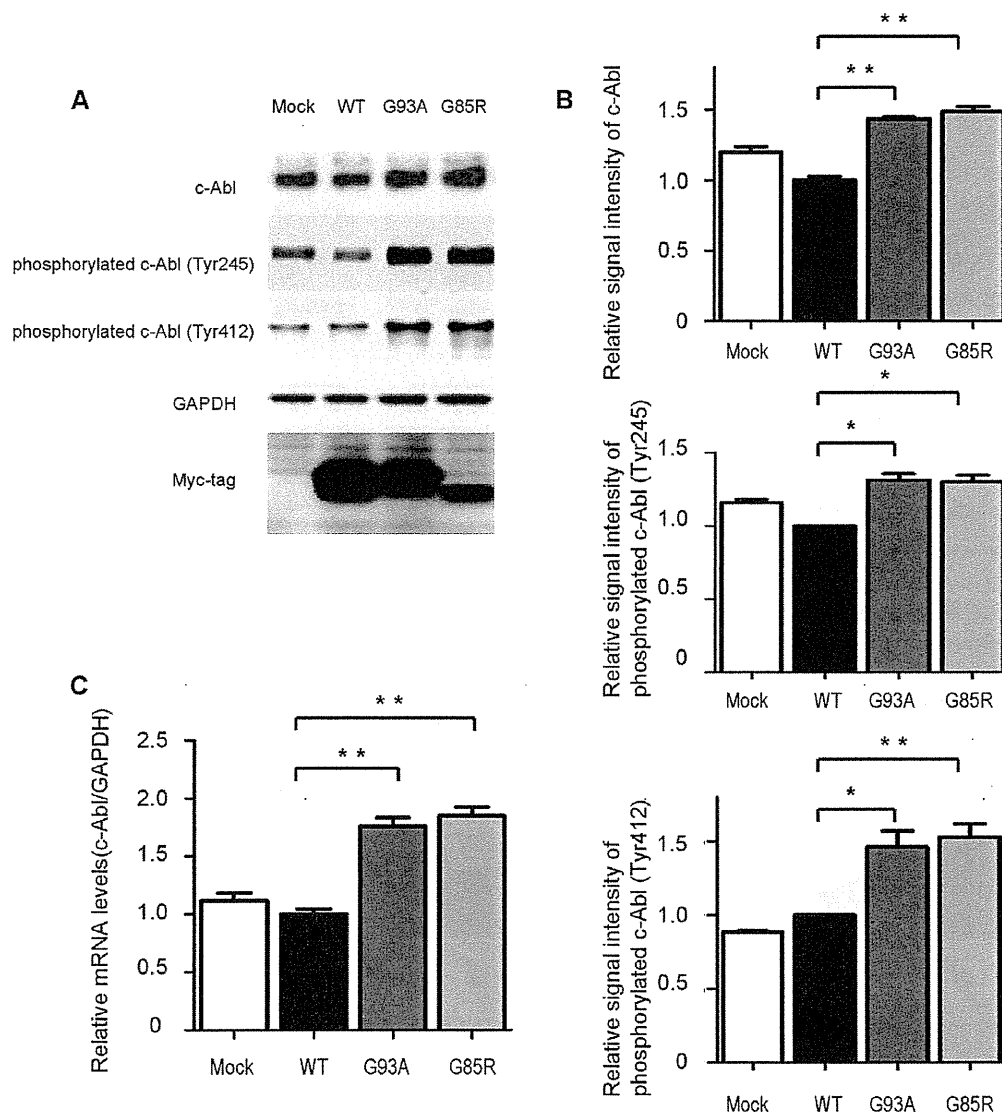


Figure 2. Activation of c-Abl caused by mutant SOD1 overexpression. A: Total c-Abl and phospho-c-Abl (Tyr245 and Tyr412) protein levels in NSC-34 cells overexpressing human wild-type and mutant SOD1 protein were measured by western blotting. GAPDH is shown as a loading control. Cells were cultured with doxycycline (Dox, 2 $\mu\text{g}/\text{ml}$) in serum-free culture medium for 48 h. B: Densitometric analysis ($n=3$ per group) of the results shown in Fig. 2A demonstrated that both types of mutant SOD1, G93A and G85R, significantly increased the amount of total c-Abl protein and facilitated phosphorylation at both c-Abl sites, Tyr245 and Tyr412. Data are presented as mean \pm SEM. Statistical analysis was performed using 1-way ANOVA with Dunnett's post-hoc test. $*P<0.05$, $**P<0.01$. C: Expression levels of c-Abl mRNA were measured by quantitative RT-PCR in NSC-34 cells overexpressing wild-type or mutant human SOD1 ($n=4$ per group). Cells were cultured with doxycycline (Dox, 2 $\mu\text{g}/\text{ml}$) in serum-free culture medium for 48 h. Overexpression of both types of mutant SOD1 significantly increased the c-Abl mRNA level compared with overexpression of wild-type SOD1 ($P<0.01$). Data shown are ratios (mean \pm SEM) of the c-Abl mRNA levels in NSC-34 cells overexpressing wild type SOD1 ($n=6$). Statistics were evaluated using 1-way ANOVA with Dunnett's post-hoc test. $**P<0.01$. doi:10.1371/journal.pone.0046185.g002

Dasatinib reduces phosphorylation of c-Abl and the activated form of caspase-3 in G93A mice

To assess the effect of dasatinib on the central nervous system (CNS), we performed western blot analyses using the spinal cords of G93A mice and control littermates treated with dasatinib or vehicle (Fig. 7). The levels of phosphorylated c-Abl (Tyr245) were decreased in a dose-dependent manner in G93A mice treated with dasatinib. In addition, activated caspase-3 was decreased in mice treated with high-dose dasatinib (Fig. 7). Quantification of

immunofluorescence revealed that phosphorylated c-Abl (Tyr412) levels were significantly decreased in dasatinib-treated G93A mice at doses of 15 $\text{mg}/(\text{kg}\cdot\text{day})$ or higher compared with vehicle-treated control mice ($P<0.01$) (Fig. S2). These results suggest that dasatinib protects motor neurons from mutant SOD1-induced neuronal cell death by inhibiting apoptosis.

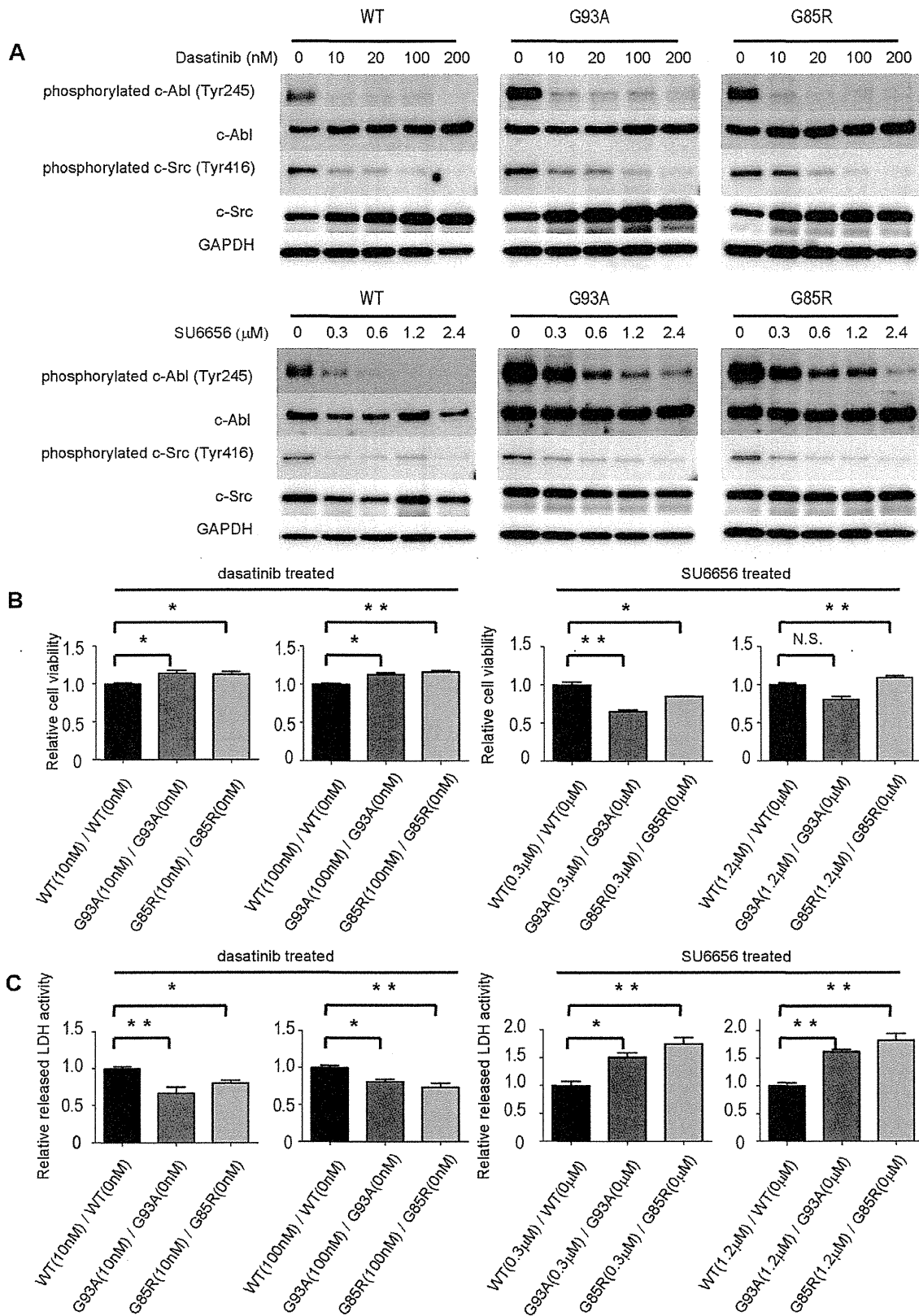


Figure 3. Dasatinib reduces cytotoxicity of mutant SOD1s in NSC-34 cells. A: Protein levels of phosphorylated c-Abl (Tyr245), c-Abl, phosphorylated c-Src (Tyr416), c-Src, and GAPDH in NSC-34 cells overexpressing human wild-type or mutant SOD1s treated with various concentrations of dasatinib or SU6656 were measured by western blot. Cells were cultured in serum-free culture medium with doxycycline (Dox, 2 $\mu\text{g}/\text{ml}$), and western blot was performed at 24 h after dasatinib or SU6656 addition. B: Cells were grown in 96-well collagen-coated plates (3,500 cells per well) with doxycycline (Dox, 2 $\mu\text{g}/\text{ml}$) in culture medium containing 10% FBS for 16 h. Culture medium was then replaced with 1% FBS-containing medium including the indicated concentrations of dasatinib and 2 $\mu\text{g}/\text{ml}$ doxycycline (Dox). MTS assays were performed at 24 h after addition of dasatinib or SU6656. Viability was measured as the level of absorbance at 490 nm. Absorbance at 490 nm was expressed as the mean \pm SEM (n = 6). Ratios of relative cell viability based on the MTS assay were calculated to determine the beneficial effect of dasatinib in mutant cells overexpressing SOD1s. Absorbance at 490 nm was standardized relative to the absorbance at each corresponding time point for 0 nM dasatinib. Cell viability assay confirmed that dasatinib significantly reduced the cytotoxicity of mutant SOD1s, whereas SU6656 did not. Statistics were evaluated using 1-way ANOVA with Dunnett's post-hoc test. * $P < 0.05$, ** $P < 0.01$. C: Cells were grown in 96-well collagen-coated plates (3,500 cells per well) with doxycycline (Dox, 2 $\mu\text{g}/\text{ml}$) in culture medium containing 10% FBS for 16 h. Culture medium was then replaced with 1% FBS-containing medium with the indicated concentrations of dasatinib and 2 $\mu\text{g}/\text{ml}$ doxycycline (Dox). LDH assays were performed at 24 h after dasatinib or SU6656 addition. Cytotoxicity was measured as the level of absorbance at 490 nm. Ratios of relative LDH release were calculated to determine the beneficial effect of dasatinib in mutant cells overexpressing SOD1s. Absorbance at 490 nm was standardized relative to the absorbance at each corresponding time point for 0 nM dasatinib. LDH assay confirmed that dasatinib significantly reduced the cytotoxicity of mutant SOD1s, whereas SU6656 did not. Values represent the mean \pm SEM of the ratio of LDH release (n = 4). Statistics were evaluated using 1-way ANOVA with Dunnett's post-hoc test. * $P < 0.05$, ** $P < 0.01$. doi:10.1371/journal.pone.0046185.g003

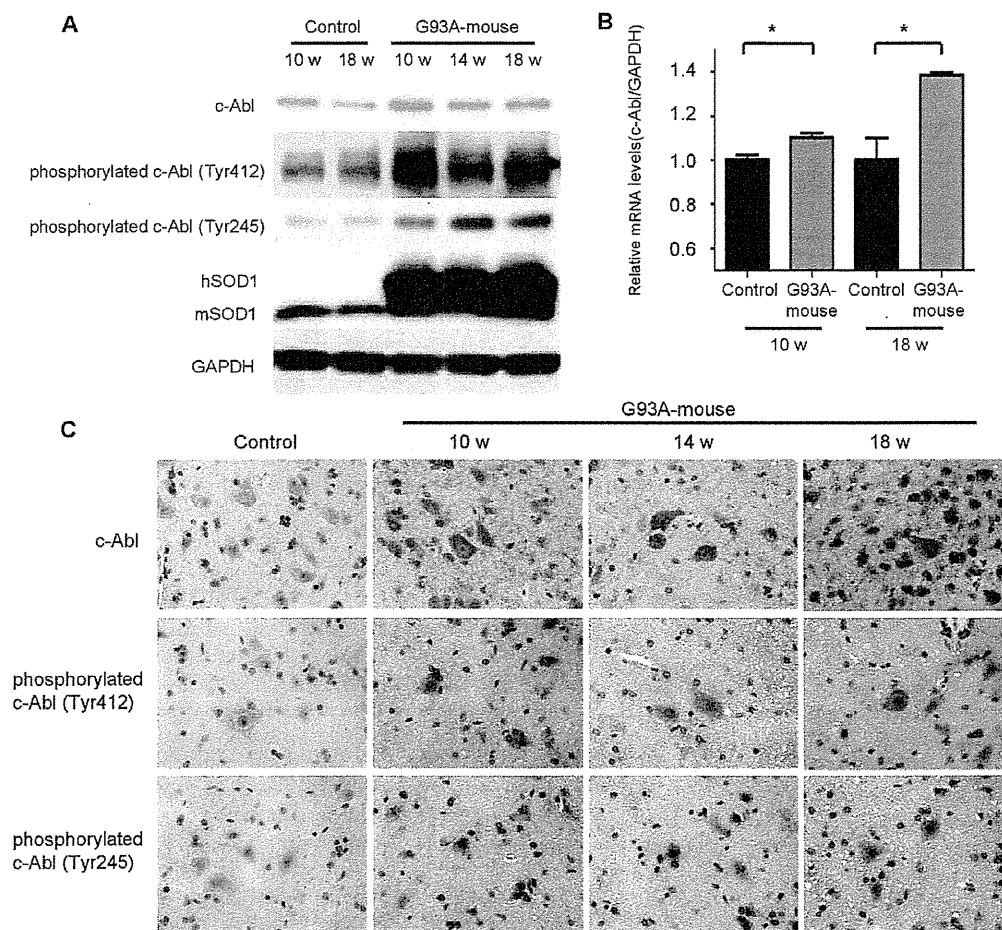


Figure 4. c-Abl upregulation and activation in G93A mice. A: Protein levels of phosphorylated c-Abl (Tyr245 and Tyr412) and c-Abl were analyzed by western blot using spinal cord protein extracts from control non-transgenic and G93A mice at the indicated ages. GAPDH is shown as a loading control. hSOD1 and mSOD1 indicate human SOD1 and mouse endogenous SOD1, respectively. B: c-Abl mRNA levels in the spinal cords of G93A mice and control littermates (age 10 and 18 weeks; n = 4 per group) were measured by quantitative RT-PCR. Data shown are the ratios of the c-Abl mRNA level in each group relative to that in control littermates. c-Abl mRNA was significantly increased in the spinal cords of G93A mice in both age groups compared with control littermates ($P < 0.05$). Data are presented as mean \pm SEM. Statistics were evaluated using Student's *t* test. * $P < 0.05$. C: Distribution of total and phosphorylated c-Abl proteins was analyzed by immunohistochemical staining of paraffin-embedded spinal cord sections from G93A mice (10, 14, and 18 weeks old) and control littermates (20 weeks old) using antibodies directed against c-Abl, phosphorylated c-Abl (Tyr245), and phosphorylated c-Abl (Tyr412). Scale bar: 50 μm . doi:10.1371/journal.pone.0046185.g004

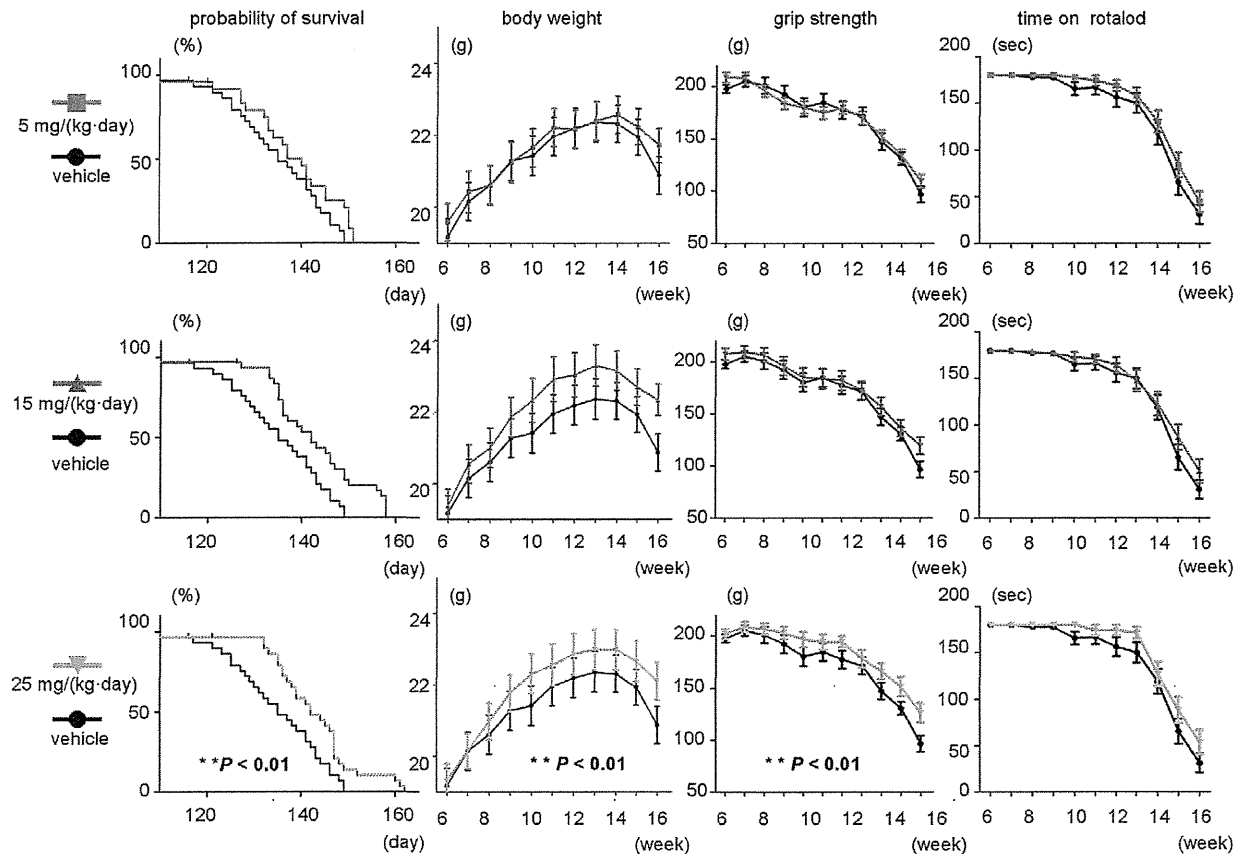


Figure 5. The effect of dasatinib on survival and disease progression in G93A mice. Rotarod activity, grip strength, body weight, and survival rate in G93A mice with or without dasatinib treatment (0, 5, 15, and 25 mg/(kg-day)). Survival of G93A mice was improved by dasatinib at a dose of 25 mg/(kg-day) compared with vehicle treatment (Log-rank test, $P < 0.01$, 25 mg/(kg-day) vs. vehicle), whereas a lower dose of dasatinib (5 mg/(kg-day)) had no significant effect on life span. Weight loss was also ameliorated by dasatinib at a dose of 25 mg/(kg-day) compared with vehicle treatment (2-way ANOVA, $P < 0.01$, 25 mg/(kg-day) vs. vehicle). The administration of dasatinib at 25 mg/(kg-day) similarly ameliorated grip strength (2-way ANOVA, $P < 0.01$, 25 mg/(kg-day) vs. vehicle). The difference in physical function between the groups as assessed by rotarod was not significant by 2-way ANOVA, although a beneficial tendency of dasatinib was observed.
doi:10.1371/journal.pone.0046185.g005

Upregulation and activation of c-Abl in sporadic ALS

To investigate the implications of c-Abl in human sALS, we next examined the expression and activation levels of c-Abl in post-mortem spinal cord specimens from sALS cases. Lumbar spinal cord tissue from 3 sALS cases and 3 control cases with no neurodegenerative disease were used for immunohistochemical and western blot analyses. Western blotting revealed a more than 3-fold increase in c-Abl protein in sALS (Fig. 8A, B). More intense c-Abl immunohistochemical signal was also observed in lumbar spinal cord sections from sALS cases compared to control cases (Fig. 8C). Immunoreactivity of phosphorylated c-Abl (Tyr245 and Tyr412) in motor neurons was also increased in sALS specimens compared to controls (Fig. 8C). These findings indicate that upregulation and activation of c-Abl in motor neurons occurs not only in G93A mice but also in sALS patients.

Discussion

In this study, we established mouse motor neuronal cell lines in which either wild-type or mutant SOD1s were induced by doxycycline. We found that overexpression of mutant SOD1s induced expression and activation of c-Abl and decreased cell

viability in a mouse motor neuron cell model. Furthermore, dasatinib, a BBB-permeable inhibitor of c-Abl, attenuated c-Abl phosphorylation and reduced the cytotoxicity induced by overexpression of mutant SOD1s. Dasatinib is a dual kinase inhibitor against c-Abl and c-Src family tyrosine kinases [31]. To clarify the specificity of c-Abl for the motor neuronal cytotoxicity, we performed cell proliferation and cell death assays with or without SU6656, which preferentially inhibits c-Src compared to c-Abl [32]. As shown in Fig. 3, dasatinib ameliorated the cytotoxic effects of mutant SOD1, whereas SU6656 did not. This finding indicates that c-Abl inhibition delays motor neuronal cell death caused by mutant SOD1. Our results are consistent with previous studies demonstrating that some apoptotic stimuli, such as amyloid beta and oxidative stress, also caused c-Abl activation [25,29], and that imatinib, another c-Abl inhibitor, had an inhibitory effect on apoptotic pathways [28].

Our study also provides evidence that c-Abl upregulation and activation occur in the lumbar spinal cord of G93A mice. c-Abl activation has recently been reported to occur in animal models of Niemann-Pick type C and Alzheimer's disease [28,33], but the present report is the first to demonstrate c-Abl activation in an animal model of ALS. Throughout the disease course of G93A

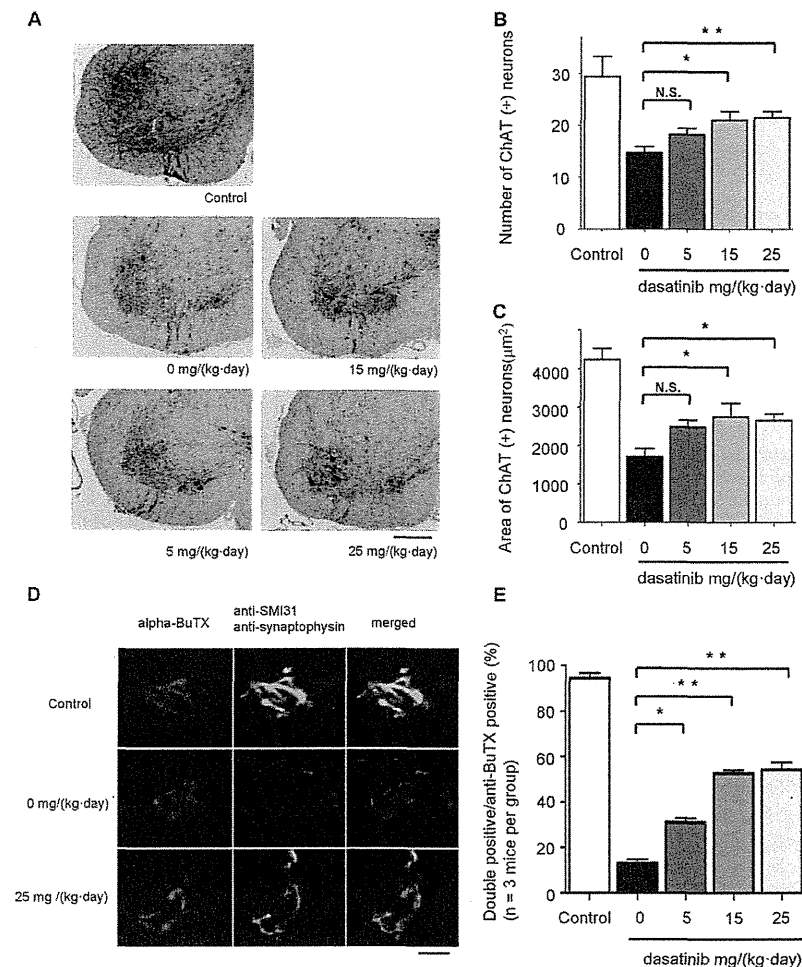


Figure 6. The effect of dasatinib on motor neuron survival in G93A mice. A: Spinal cord (L1-3) specimens from 120-day-old mice were immunostained with anti-ChAT antibody. The mice were administered the indicated amounts of dasatinib daily from postnatal day 56 to day 120 ($n = 8$ mice per group). Scale bar: 250 μm . B: The number of ChAT-positive neurons in the sections described in Fig. 6A was counted using Image J software. Dasatinib prevented the loss of ChAT-positive motor neurons in the ventral horn of G93A mice at doses of 15 mg/(kg-day) ($P < 0.05$) and 25 mg/(kg-day) ($P < 0.01$). Statistics were evaluated using 1-way ANOVA with Dunnett's post-hoc test. $*P < 0.05$, $**P < 0.01$. C: The area of ChAT-positive neurons in the sections described in Fig. 6A was determined using Image J software. Dasatinib increased the size of motor neuron cell bodies at doses of 15 and 25 mg/(kg-day) ($P < 0.05$). Statistics were evaluated using 1-way ANOVA with Dunnett's post-hoc test. $*P < 0.05$. D: To investigate the innervation status of NMJs, frozen quadriceps femoris specimens from 120-day-old mice were stained with alpha-BuTX (red) and anti-synaptophysin (green) or anti-SMI31 (green) antibodies. Representative NMJs visualized with the confocal laser scanning microscopy are shown. The mice were administered the indicated amounts of dasatinib daily from postnatal day 56 to day 120. Scale bar: 10 μm . E: The ratio of double-immunostained innervated NMJs to total NMJs is summarized. One hundred immunostained NMJs were investigated in each dasatinib-treated mouse ($n = 3$ mice per group). Dasatinib significantly ameliorated the destruction of NMJ innervation in G93A mice at doses of 5 ($P < 0.05$), 15, and 25 mg/(kg-day) ($P < 0.01$). Statistics were evaluated using 1-way ANOVA with Dunnett's post-hoc test. $*P < 0.05$, $**P < 0.01$. doi:10.1371/journal.pone.0046185.g006

mice, hyperphosphorylation and upregulation of c-Abl was apparent in the lumbar spinal cord. Notably, although apoptosis-related molecules such as c-Abl were expected to exert their function at a relatively late stage of disease [34,35], the expression of c-Abl was increased at the presymptomatic stage. This unexpected result suggests that c-Abl may be an early player in the apoptotic cascade of ALS pathogenesis and thus a promising target to protect motor neurons against cytotoxic insults.

The currently available c-Abl inhibitors are imatinib, dasatinib, and nilotinib, all of which have been used for the treatment of CML, Ph+ALL, and gastrointestinal stromal tumor [36,37,38]. A number of studies have reported CNS relapse in patients treated

with imatinib, which has poor BBB permeability [39,40,41,42,43,44], while in contrast, Porkka et al. reported that dasatinib crossed the BBB and showed therapeutic efficacy against CNS CML tumors in a mouse model and in patients with CNS leukemia (Ph+ALL) [45]. The high BBB permeability of dasatinib is advantageous for the treatment of ALS, since it is expected to achieve a sufficient therapeutic concentration in the CNS. We demonstrated that dasatinib at a dose of 15 mg/(kg-day) or more delayed disease progression and extended the survival of G93A mice. Immunostaining of spinal cords clearly demonstrated a dose-dependent protective effect of dasatinib on motor neuron survival by inhibiting apoptosis. These results indicate that c-Abl plays an

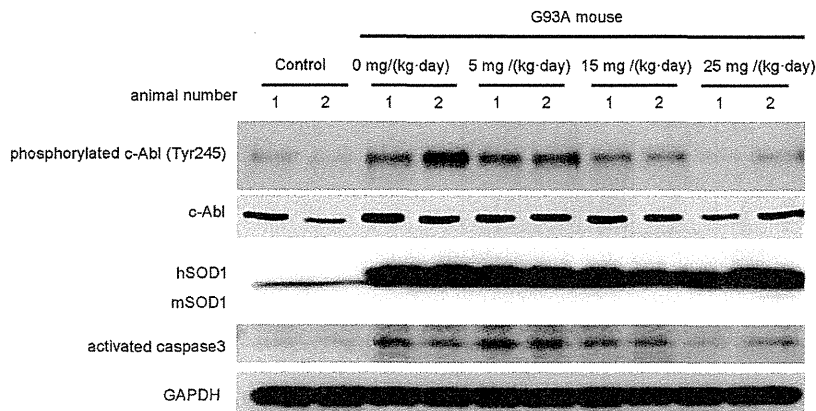


Figure 7. Dasatinib inhibits c-Abl phosphorylation in G93A mice. Protein levels of phosphorylated c-Abl (Tyr245), c-Abl, and activated caspase-3 were measured by western blot analysis using spinal cords from dasatinib- and vehicle-treated G93A mice (120 days old). GAPDH is shown as the loading control. hSOD1 and mSOD1 indicate human SOD1 and mouse endogenous SOD1, respectively. Western blot analysis is shown in duplicate. The animal number refers to individual animals. Parallel declines in c-Abl phosphorylation and activated caspase 3 were observed. doi:10.1371/journal.pone.0046185.g007

important role in the disease pathogenesis of ALS in G93A mice and is a promising therapeutic target for ALS.

Since the involvement of c-Abl upregulation and activation has been demonstrated in neuronal cell apoptosis [46,47], we investigated whether upregulation of c-Abl is associated with an increased level of activated caspase-3, which correlates with apoptosis. Our results clearly showed that caspase 3 was activated in the spinal cords of G93A mice. Administration of dasatinib attenuated both c-Abl phosphorylation and caspase-3 activation in a dose-dependent manner. Thus, our results suggest that dasatinib ameliorates the phenotype of these animals by suppressing apoptotic cell death of motor neurons caused by mutant SOD1.

The examination of NMJs revealed that dasatinib successfully reversed the denervation of NMJs, an early pathological change reflecting motor neuron degeneration in mutant SOD1-mediated ALS [48]. Since levels of total and active c-Abl were increased in the spinal cords of G93A mice at the early stage of the disease (Fig. 4), dasatinib appears to improve NMJ function via c-Abl-mediated signaling. These findings suggest that dasatinib improved motor neuron function leading to amelioration of weight loss in G93A mice. They also demonstrate that the loss of synaptic contacts is a sensitive indicator of the beneficial effects exerted by dasatinib in G93A mice.

One possible explanation for the relatively small effects of dasatinib in this study is that the beneficial effects of this therapy on apoptosis were limited in motor neurons and could not reverse the physical dysfunction of the mice, despite the improvement in innervation at NMJs. Alternatively, dasatinib may not be capable of mitigating non-apoptotic pathways of motor neuron degeneration caused by mutant SOD1, since non-apoptotic programmed cell death has also been implicated in motor neuron damage in G93A mice [49]. Taken together, dasatinib may mitigate apoptotic events that occur at an early stage of the disease and partially improve motor neuron function via activation of c-Abl.

Using human postmortem spinal cord tissue, we demonstrated a significant increase in c-Abl expression in the spinal cord of sALS compared with non-ALS. Histochemical findings confirmed that c-Abl protein increased mainly in motor neurons. In addition, c-Abl phosphorylation was also increased in motor neurons in the affected area. These findings indicate that c-Abl abnormality is involved in human sALS cases as well as cellular and animal

models of ALS. Thus far, not many drug candidates derived from research using mutant SOD1 transgenic animals have been successful in clinical trials for human sALS [50]. The implication of c-Abl in sALS as well as mutant SOD1-associated ALS supports the possible application of dasatinib as a candidate drug for sALS treatment. Our study showed that dasatinib treatment suppressed apoptosis and delayed disease progression in G93A mice, suggesting that dasatinib has a potential therapeutic value in humans, since apoptosis appears to be an important target of treatment development for ALS [35,51].

In conclusion, the major findings of this study are (1) the observation of c-Abl upregulation and activation in the spinal cords of G93A mice at a relatively early stage of the disease; (2) the improved survival of G93A mice with concomitant suppression of c-Abl phosphorylation and caspase-3 activation upon administration of a BBB-permeable c-Abl inhibitor, dasatinib; and (3) increased c-Abl expression and phosphorylation in postmortem spinal cord tissues from sALS patients. Taken together, our results suggest that c-Abl is a novel therapeutic target for ALS.

Materials and Methods

Cell lines

The mouse motor neuron hybridoma line NSC-34 was provided by Dr. N.R. Cashman (University of Toronto; Toronto, Canada) [30]. Human wild-type and mutant (G93A and G85R) SOD1 cDNAs were subcloned from pcDNA3.1/SOD1 into lentiviral expression vectors (pLenti-CMV/TO, kind gifts from Dr. Eric Campeau at the University of Massachusetts Medical School) [52]. Lentiviral particles were produced in HEK293T cells (Open Biosystems, Huntsville, AL, USA) by transfection with Lipofectamine 2000 (Invitrogen, Eugene, OR, USA). Lentivirus-containing supernatant was collected 48 h after transfection and stored at -80°C . Details of the lentivirus system have been described previously [52]. We first transduced the Tet repressor into NSC-34 cells and selected a single clone (NSC-34-TetR14) that demonstrated good induction without leaky expression. NSC-34-TetR14 cells were stably transduced with lentivirus-Tet-on/SOD1, an inducible lentivirus expressing Myc-tagged wild-type or mutant SOD1.

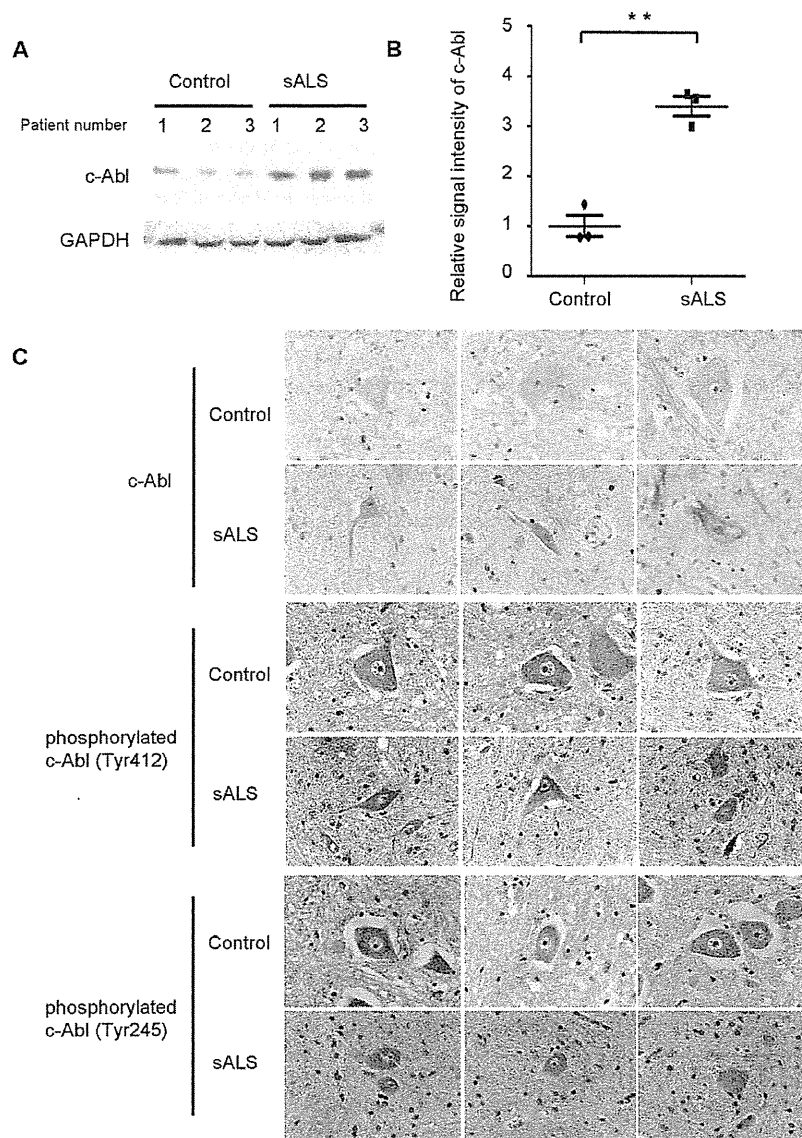


Figure 8. c-Abl upregulation and activation in affected motor neurons of sporadic ALS patients. A: The protein expression of total c-Abl was measured by western blot analysis using an anti-c-Abl antibody and the lumbar spinal cord tissue from sporadic ALS (sALS) cases and controls. GAPDH is shown as an internal control. The patient number refers to individual patients. B: Densitometric analysis using Image J software revealed a significant difference in the amount of total c-Abl protein in the lumbar spinal cords of sALS patients and controls ($P < 0.01$). Data are presented as mean \pm SEM. Statistical analysis was performed using Student's *t* test. $**P < 0.01$. C: Immunohistochemical analysis using paraffin-embedded spinal cords from control and sALS patients was carried out by staining with anti-c-Abl, anti-phosphorylated c-Abl (Tyr412), and anti-phosphorylated c-Abl (Tyr245) antibodies. Scale bar: 50 μ m. doi:10.1371/journal.pone.0046185.g008

Cell culture

NSC-34 cells were grown in Dulbecco's modified Eagle's medium (DMEM) containing 10% fetal calf serum (FCS; Invitrogen). The tet-on inducible cell lines were grown in DMEM supplemented with 10% tetracycline-free FCS (Clontech, Mountain View, CA, USA). All cell lines used in this study were cultured at 37°C in an atmosphere of 5% CO₂. We induced hSOD1 expression by adding 2 μ g/ml doxycycline (Clontech) to the culture medium for the last 48 h of culture.

Cell viability assay

Each of the cell lines (3,500 cells per well) were grown on collagen-coated 96-well plates with serum-free medium. MTS (3-(4,5-dimethylthiazol-2-yl)-5-(3-carboxymethoxyphenyl)-2-(4-sulphophenyl)-2H-tetrazolium)-based cell proliferation assays were performed after 48 h of induction with doxycycline (Dox, 2 μ g/ml) using the CellTiter 96[®] AQueous One Solution Cell Proliferation Assay (Promega, Madison, WI, USA). Briefly, we added CellTiter 96[®] AQueous One Solution Reagent to each well of a 96-well assay plate containing the samples in culture medium. After incubation at 37°C for 1 h, absorbance at 490 nm was measured

using a multiple-plate reader (Powerscan HT, Dainippon Pharmaceutical, Osaka, Japan), with assays carried out in triplicate.

Cytotoxicity detection assay

Cell injury was quantitatively assessed by measurement of LDH released from damaged or destroyed cells into the extracellular fluid after 48-h induction of wild-type or mutant SOD1. The activity of LDH released into the culture medium was measured with a Cytotoxicity Detection kit (Roche Applied Science, Burgess Hill, UK) according to the manufacturer's protocol. Briefly, after 48 h of induction with doxycycline (Dox, 2 $\mu\text{g}/\text{ml}$), we added substrate mixture from the kit to each well of a 96-well assay plate containing the culture supernatant. Following incubation for 30 min, absorbance at 490 nm was measured using a multiple-plate reader (Powerscan HT, Dainippon Pharmaceutical, Osaka, Japan).

Transgenic mice

Transgenic mice overexpressing the human SOD1 gene carrying the G93A mutation were purchased from the Jackson Laboratory (Bar Harbor, ME, USA) and maintained as hemizygotes by mating transgenic males with B6/SJLFl females [53]. All animal experiments were performed in accordance with the National Institute of Health Guide for the Care and Use of Laboratory Animals and were approved by the Nagoya University Animal Experiment Committee.

Chemicals

Dasatinib was provided by Bristol-Myers Squibb. Propylene glycol was purchased from Sigma Chemical Co. (St Louis, MO, USA). SU6656 was purchased from Calbiochem (Darmstadt, Germany). All other chemicals used were reagent grade or better.

Drug formulation and administration

For oral administration, dasatinib was dissolved in a mixture of propylene glycol/water (50:50). The administration volume was 0.01 ml/g. Ludolph et al. recommended that a total of 48 G93A mice should be used in a preclinical trial if 2 groups (treated animals and controls; $n = 24$ per group) are to be compared, and recommended that the number of animals should be increased for testing the dose-response effect of a drug [50]. Therefore, we allocated 28 mice to each treatment group for the survival analysis. From postnatal day 56, dasatinib was administered by oral gavage using a 5-days-on/2-days-off once-daily schedule (Monday through Friday) at doses of 5, 15, and 25 mg/(kg·day). Control mice received vehicle alone.

Immunohistochemistry

Under pentobarbital anesthesia, mice were transcardially perfused with 20 ml phosphate buffer (pH 7.4). Tissues were postfixed overnight in 10% phosphate-buffered formalin and processed for paraffin embedding as previously described [54]. Transverse sections of spinal cord (6- μm thickness) were then deparaffinized with alcohol, rehydrated, and microwaved in 0.1 M citrate buffer (pH 6) as a pretreatment for antigen retrieval. Immunostaining was performed using the EnVision+ System-HRP (Dako, Glostrup, Denmark). Tissue sections were incubated with anti-c-Abl antibody (Abcam, Cambridge, MA) and anti-phospho-c-Abl (Tyr412 or Tyr245) antibody (Cell Signaling Technology, Beverly, MA, USA), both diluted 1:100 in Dako antibody diluent (Dako) for immunohistochemical analysis. Counterstaining was performed using hematoxylin. For fluorescence microscopic analysis, after antigen retrieval, tissue sections were incubated

with TNB-buffer (0.10 M Tris-HCl, 0.15 M NaCl, 0.5% BMP) for 30 min at room temperature to block non-specific antibody binding. Then spinal tissue sections were incubated with anti-phospho-c-Abl (Tyr412 or Tyr245) antibody (Cell Signaling Technology), both diluted 1:100 in phosphate buffered saline (PBS) buffer, overnight at 4°C. After incubation with primary antibody, the sections were exposed to an appropriate secondary antibody conjugated to fluorescent dye and Topro-3 (Invitrogen) for 1 h at room temperature. Sections were visualized using a confocal microscope (LSM 710, Carl Zeiss, Oberkochen, Germany) under epifluorescent illumination. The intensity of immunostained neurons was semi-quantified using NIH Image J software (v 1.44, NIH, Bethesda, MD, USA).

Assessment of motor function

The motor performance of mice was assessed weekly using an Economex Rotarod (Columbus Instruments, Columbus, OH, USA) starting at 42 days of age. Staying on the rod for more than 180 s was considered to be the normal performance level, as previously described [55].

Western blot analyses

The spinal cords of dasatinib- and vehicle-treated mice were collected approximately 3 h after the final oral administration. Human and mouse spinal cords were snap frozen in liquid nitrogen, homogenized in ice-cold Cell Lysis-M Mammalian Cell Lysis/Extraction Reagent (Sigma), and centrifuged at $18,800 \times g$ for 15 min at 4°C. Protein concentration was determined by DC protein assay (Bio-Rad, Hercules, CA, USA). Western blotting was performed using standard procedures as described previously [56,57]. Primary antibodies were used at the following concentrations: anti-SOD1, 1:2,000 (Abcam); anti-Myc, 1:1,000 (MBL, Nagoya, Japan); anti-tubulin, 1:1,000 (Sigma); anti-c-Abl, 1:1,000 (BD Transduction); anti-phospho-c-Abl (Tyr412), 1:1,000 (Sigma); anti-phospho-c-Abl (Tyr245), 1:1000 (Cell Signaling Technology); anti-glyceraldehyde-3-phosphate dehydrogenase (GAPDH), 1:1,000 (Millipore, Billerica, MA); anti-phospho-c-Src (Tyr416), 1:1,000 (Cell Signaling Technology); anti c-Src, 1:1,000 (Cell Signaling Technology); and anti-cleaved caspase-3 (Asp175), 1:1,000 (Cell Signaling Technology). Secondary antibody probing and detection were performed using the ECL Plus kit (GE Healthcare, Buckinghamshire, UK). For detection of phosphorylated c-Abl, antibody was diluted in Tris-buffered saline (TBS) with Tween (0.5%) containing 3% BSA, otherwise 5% fat-free milk in TBS with Tween (0.5%) was used as the antibody diluent. Chemiluminescence signals were digitalized (LAS-3000 Imaging System; Fujifilm, Tokyo, Japan), and band intensities were quantified using Multi Gauge software version 3.0 (Fujifilm).

Quantitative real-time PCR

Real-time PCR was performed as described previously [58]. In brief, total RNA from either mouse spinal cord or NSC-34 cells was reverse transcribed into first-strand cDNA using SuperScript II reverse transcriptase (Invitrogen). Real-time PCR was performed using QuantiTect SYBR Green PCR Master Mix and 0.4 M of each primer (Qiagen, Valencia, CA, USA), and the product was detected using the CFX96™ real-time system (Bio-Rad Laboratories). The reaction conditions were 95°C for 15 min, followed by 40 cycles of 15 s at 94°C, 30 s at 55°C, and 30 s at 72°C. The expression level of GAPDH was quantified and used as an internal standard control. The primers used were 5'-TCGTTACCTCCAAAGGCTGCTC-3' and 5'-ATGGCGGTGTCTGGCTATTCA-3' for c-Abl and 5'-TCAA-

GAAGGTGGTGAAGCAG-3' and 5'-GTTGAAGTCGCAG-GAGACAA-3' for GAPDH.

Motor neuron assessment by immunohistochemical analysis

At age 120 days, 8 animals from each treatment group were sacrificed, and the lumbar spinal cords (L1-3) were collected. The samples were embedded in paraffin, and 6- μ m sections were prepared. Spinal cord tissue sections were immunostained with anti-ChAT antibody (Millipore) diluted 1:1,000 in Dako antibody diluent (Dako) using the EnVision+ System-HRP (Dako). ChAT-immunoreactive neurons in the ventral horn of the lumbar spinal cord (L1-3) were counted in 3 sections taken at 60- μ m intervals, and the mean total number of ChAT-immunoreactive neurons was compared between treatment groups. The area (pixels) of ChAT-immunoreactive neurons was analyzed using NIH Image J software (NIH). ChAT-positive cells with an area greater than 100 μ m² were presumed to be motor neurons.

NMJ assessment by immunohistochemical analysis

At the age of 120 days, 8 animals from each treatment group were sacrificed, and quadriceps femoris specimens were quickly frozen in liquid nitrogen. The samples were mounted in Tissue-Tek OCT compound (Sakura, Tokyo, Japan), and 30- μ m cryostat sections were prepared from the frozen tissues. Frozen sections were fixed in acetone for 5 min and then incubated with TNB-buffer (0.10 M Tris-HCl, 0.15 M NaCl, 0.5% BMP) for 15 min at room temperature to block non-specific antibody binding. Sections were incubated with primary antibodies and alpha-BuTX overnight at 4°C. The following primary antibodies were used: anti-synaptophysin diluted 1:100 (Cell Signaling Technology) and anti-SMI31, 1:100 (COVANCE, Princeton, NJ, USA). Alpha-BuTX biotin-XX-conjugate diluted 1:80 was purchased from Molecular Probes (Eugene, OR, USA). After washing with PBS, the sections were exposed to appropriate secondary antibody and streptavidin-conjugated fluorescent dye for 1 h at room temperature, then washed with PBS again and mounted. Sections were examined and photographed using a confocal microscope (LSM 710, Carl Zeiss) under epifluorescent illumination.

Human sporadic ALS samples

Spinal cord specimens were obtained at autopsy from 3 pathologically confirmed cases of sALS (2 men, aged 71 and 73 y, and 1 woman, aged 53 y) and 3 cases of non-neurodegenerative disease. Lumbar spinal cord tissue was either homogenized for western blot analysis or embedded in paraffin for immunohistochemical analysis. The collection of autopsied human tissues and their use for this study were approved by the Ethics Committee of Nagoya University Graduate School of Medicine, and written informed consent was obtained from the patients' next-of-kin. Experimental procedures involving human subjects were conducted in conformance with the principles expressed in the Declaration of Helsinki.

Statistical analyses

Statistical analyses were performed using Prism software (GraphPad Software, La Jolla, CA, USA). Biochemical data were statistically analyzed using Student's t test or 1-factor factorial ANOVA followed by appropriate post-hoc tests. Survival data was

analyzed by log-rank tests, and body weight change was analyzed by 2-factor factorial ANOVA. *P* values of 0.05 or less were considered to be statistically significant.

Supporting Information

Figure S1 Increased phosphorylated c-Abl in spinal cords of G93A mice. A: The distribution of phosphorylated c-Abl proteins was analyzed by immunohistochemical staining of paraffin-embedded spinal cord sections from G93A mice (10, 14, and 18 weeks old) and control littermates (20 weeks old) using antibodies directed against phosphorylated c-Abl (Tyr245 and Tyr412). The spinal sections were immunostained with anti-ChAT (red) and anti-phosphorylated c-Abl (Tyr245 or Tyr412) (green) antibodies together with Topro-3 (blue). Representative immunostained motor neurons visualized with confocal laser scanning microscopy are shown. Scale bar: 50 μ m. B: The intensity of motor neurons labeled with anti-phosphorylated c-Abl (Tyr245) and anti-phosphorylated c-Abl (Tyr412) antibodies shown in A was quantified (*n* = 3 mice per group). Phosphorylated c-Abl immunoreactivity with both antibodies was significantly increased in the spinal cords of G93A mice (*P* < 0.01). The value was standardized to that of the fluorescence intensity of control mice. Statistics were evaluated using 1-way ANOVA with Dunnett's post-hoc test. ***P* < 0.01. (TIF)

Figure S2 Dasatinib reduced c-Abl phosphorylation (Tyr412) in G93A mice. A: Phosphorylated c-Abl (Tyr412) protein was analyzed by immunohistochemical staining of paraffin-embedded spinal cord sections from dasatinib-treated G93A mice (0, 5, 15, and 25 mg/(kg·day)) using an antibody against phosphorylated c-Abl (Tyr412). The spinal sections were fluorescently immunostained with anti-ChAT (red) and anti-phosphorylated c-Abl (Tyr412) (green) antibodies together with Topro-3 (blue). Representative immunostained motor neurons visualized with confocal laser scanning microscopy are shown. Scale bar: 50 μ m. B: The intensity of the cells stained with anti-phosphorylated c-Abl (Tyr412) was quantified. The mice were administered the indicated amounts of dasatinib daily from postnatal day 56 to day 120 (*n* = 3 mice per group). Immunoreactivity against phosphorylated c-Abl (Tyr412) was significantly decreased in dasatinib-treated G93A mice (15 mg/(kg·day) or more) compared to vehicle-treated G93A mice (*P* < 0.01, 15 mg/(kg·day) and 25 mg/(kg·day)). The value was standardized to that of the fluorescence intensity of vehicle-treated G93A mice. Statistics were evaluated using 1-way ANOVA with Dunnett's post-hoc test. ***P* < 0.01. (TIF)

Acknowledgments

NSC-34 cells were kindly provided by Dr. N. Cashman. We thank Dr. E. Campeau for providing lentiviral expression systems.

Author Contributions

Conceived and designed the experiments: RK GS. Performed the experiments: RK SI MK KK JS. Analyzed the data: RK SI MK KK JS. Contributed reagents/materials/analysis tools: RK SI MK KK ZH JS HA FT FU. Wrote the paper: RK SI MK GS.

References

1. Tyler HR, Shefner J (1991) Amyotrophic lateral sclerosis. In: Vinken PJ, Bruyn GW, Klawans HL, editors. *Handbook of Clinical Neurology*. Amsterdam: Elsevier Science Publishers BV. pp. 169–215.
2. Emery A, Holloway S (1982) Familial motor neuron diseases. In: Rowland L, editor. *Human Motor Neuron Diseases*. New York: Raven Press Ltd. pp. 139–147.
3. Rosen DR, Siddique T, Patterson D, Figlewicz DA, Sapp P, et al. (1993) Mutations in Cu/Zn superoxide dismutase gene are associated with familial amyotrophic lateral sclerosis. *Nature* 362: 59–62.
4. Martin LJ, Liu Z, Chen K, Price AC, Pan Y, et al. (2007) Motor neuron degeneration in amyotrophic lateral sclerosis mutant superoxide dismutase-1 transgenic mice: mechanisms of mitochondrialopathy and cell death. *J Comp Neurol* 500: 20–46.
5. Bruijn LI, Houseweart MK, Kato S, Anderson KL, Anderson SD, et al. (1998) Aggregation and motor neuron toxicity of an ALS-linked SOD1 mutant independent from wild-type SOD1. *Science* 281: 1851–1854.
6. Boillee S, Vande Velde C, Cleveland DW (2006) ALS: a disease of motor neurons and their nonneuronal neighbors. *Neuron* 52: 39–59.
7. Julien JP (2001) Amyotrophic lateral sclerosis: unfolding the toxicity of the misfolded. *Cell* 104: 581–591.
8. Kabashi E, Durham HD (2006) Failure of protein quality control in amyotrophic lateral sclerosis. *Biochim Biophys Acta* 1762: 1038–1050.
9. Cassina P, Cassina A, Pehar M, Castellanos R, Gandelman M, et al. (2008) Mitochondrial dysfunction in SOD1G93A-bearing astrocytes promotes motor neuron degeneration: prevention by mitochondrial-targeted antioxidants. *J Neurosci* 28: 4115–4122.
10. Jiang YM, Yamamoto M, Kobayashi Y, Yoshihara T, Liang Y, et al. (2005) Gene expression profile of spinal motor neurons in sporadic amyotrophic lateral sclerosis. *Ann Neurol* 57: 236–251.
11. Jiang YM, Yamamoto M, Tanaka F, Ishigaki S, Katsuno M, et al. (2007) Gene expressions specifically detected in motor neurons (dynactin 1, early growth response 3, acetyl-CoA transporter, death receptor 5, and cyclin C) differentially correlate to pathologic markers in sporadic amyotrophic lateral sclerosis. *J Neuropathol Exp Neurol* 66: 617–627.
12. Wang JY, Ledley F, Goff S, Lee R, Groner Y, et al. (1984) The mouse c-abl locus: molecular cloning and characterization. *Cell* 36: 349–356.
13. Nowell PC, Hungerford DA (1960) A minute chromosome in human chronic granulocytic leukemia. *Science* 132: 1488–1501.
14. Fainstein E, Marcelle C, Rosner A, Cavanaugh E, Gale RP, et al. (1987) A new fused transcript in Philadelphia chromosome positive acute lymphocytic leukaemia. *Nature* 330: 386–388.
15. Brasher BB, Van Etten RA (2000) c-Abl has high intrinsic tyrosine kinase activity that is stimulated by mutation of the Src homology 3 domain and by autophosphorylation at two distinct regulatory tyrosines. *J Biol Chem* 275: 35631–35637.
16. Sirvent A, Benistant C, Roche S (2008) Cytoplasmic signalling by the c-Abl tyrosine kinase in normal and cancer cells. *Biol Cell* 100: 617–631.
17. Pendergast AM (2002) The Abl family kinases: mechanisms of regulation and signaling. *Adv Cancer Res* 85: 51–100.
18. Zandy NL, Playford M, Pendergast AM (2007) Abl tyrosine kinases regulate cell-cell adhesion through Rho GTPases. *Proc Natl Acad Sci U S A* 104: 17686–17691.
19. Gu JJ, Ryu JR, Pendergast AM (2009) Abl tyrosine kinases in T-cell signaling. *Immunol Rev* 228: 170–183.
20. Wang JY (2000) Regulation of cell death by the Abl tyrosine kinase. *Oncogene* 19: 5643–5650.
21. Yuan ZM, Shioya H, Ishiko T, Sun X, Gu J, et al. (1999) p73 is regulated by tyrosine kinase c-Abl in the apoptotic response to DNA damage. *Nature* 399: 814–817.
22. Wang JY, Ki SW (2001) Choosing between growth arrest and apoptosis through the retinoblastoma tumour suppressor protein, Abl and p73. *Biochem Soc Trans* 29: 666–673.
23. Lu W, Finnis S, Xiang C, Lee HK, Markowitz Y, et al. (2007) Tyrosine 311 is phosphorylated by c-Abl and promotes the apoptotic effect of PKCdelta in glioma cells. *Biochem Biophys Res Commun* 352: 431–436.
24. Chen TC, Lai YK, Yu CK, Juang JL (2007) Enterovirus 71 triggering of neuronal apoptosis through activation of Abl-Cdk5 signalling. *Cell Microbiol* 9: 2676–2688.
25. Lee JH, Jeong MW, Kim W, Choi YH, Kim KT (2008) Cooperative roles of c-Abl and Cdk5 in regulation of p53 in response to oxidative stress. *J Biol Chem* 283: 19826–19835.
26. Zukerberg LR, Patrick GN, Nikolic M, Humbert S, Wu CL, et al. (2000) Cables links Cdk5 and c-Abl and facilitates Cdk5 tyrosine phosphorylation, kinase upregulation, and neurite outgrowth. *Neuron* 26: 633–646.
27. Koleske AJ, Gifford AM, Scott ML, Nee M, Bronson RT, et al. (1998) Essential roles for the Abl and Arg tyrosine kinases in neurulation. *Neuron* 21: 1259–1272.
28. Canciano GI, Toledo EM, Leal NR, Hernandez DE, Yevenes LF, et al. (2008) ST1571 prevents apoptosis, tau phosphorylation and behavioural impairments induced by Alzheimer's beta-amyloid deposits. *Brain* 131: 2425–2442.
29. Alvarez AR, Sandoval PC, Leal NR, Castro PU, Kosik KS (2004) Activation of the neuronal c-Abl tyrosine kinase by amyloid-beta-peptide and reactive oxygen species. *Neurobiol Dis* 17: 326–336.
30. Cashman NR, Durham HD, Blusztajn JK, Oda K, Tabira T, et al. (1992) Neuroblastoma x spinal cord (NSC) hybrid cell lines resemble developing motor neurons. *Dev Dyn* 194: 209–221.
31. Lombardo LJ, Lee FY, Chen P, Norris D, Barrish JC, et al. (2004) Discovery of N-(2-chloro-6-methyl-phenyl)-2-(6-(4-(2-hydroxyethyl)-piperazin-1-yl)-2-methylpyrimidin-4-ylamino)thiazole-5-carboxamide (BMS-354825), a dual Src/Abl kinase inhibitor with potent antitumor activity in preclinical assays. *J Med Chem* 47: 6658–6661.
32. Blake RA, Broome MA, Liu X, Wu J, Gishizky M, et al. (2000) SU6656, a selective src family kinase inhibitor, used to probe growth factor signaling. *Mol Cell Biol* 20: 9018–9027.
33. Alvarez AR, Klein A, Castro J, Canciano GI, Amigo J, et al. (2008) Imatinib therapy blocks cerebellar apoptosis and improves neurological symptoms in a mouse model of Niemann-Pick type C disease. *FASEB J* 22: 3617–3627.
34. Dangond F, Hwang D, Camelo S, Pasinelli P, Froesch MP, et al. (2004) Molecular signature of late-stage human ALS revealed by expression profiling of postmortem spinal cord gray matter. *Physiol Genomics* 16: 229–239.
35. Martin LJ (2010) Mitochondrial and cell death mechanisms in neurodegenerative diseases. *Pharmaceuticals (Basel)* 3: 839–915.
36. An X, Tiwari AK, Sun Y, Ding PR, Ashby CR, Jr., et al. (2010) BCR-ABL tyrosine kinase inhibitors in the treatment of Philadelphia chromosome positive chronic myeloid leukemia: a review. *Leuk Res* 34: 1255–1268.
37. Agrawal M, Garg RJ, Kantarjian H, Cortes J (2010) Chronic myeloid leukemia in the tyrosine kinase inhibitor era: what is the “best” therapy? *Curr Oncol Rep* 12: 302–313.
38. Braconi C, Bracci R, Cellerino R (2008) Molecular targets in Gastrointestinal Stromal Tumors (GIST) therapy. *Curr Cancer Drug Targets* 8: 359–366.
39. Isobe Y, Sugimoto K, Masuda A, Hamano Y, Oshimi K (2009) Central nervous system is a sanctuary site for chronic myelogenous leukaemia treated with imatinib mesylate. *Intern Med J* 39: 408–411.
40. Aichberger KJ, Herndlhofer S, Agis H, Sperr WR, Esterbauer H, et al. (2007) Liposomal cytarabine for treatment of myeloid central nervous system relapse in chronic myeloid leukaemia occurring during imatinib therapy. *Eur J Clin Invest* 37: 808–813.
41. Simpson E, O'Brien SG, Reilly JT (2006) Extramedullary blast crises in CML patients in complete hematological remission treated with imatinib mesylate. *Clin Lab Haematol* 28: 215–216.
42. Matsuda M, Morita Y, Shimada T, Miyatake J, Hirase C, et al. (2005) Extramedullary blast crisis derived from 2 different clones in the central nervous system and neck during complete cytogenetic remission of chronic myelogenous leukemia treated with imatinib mesylate. *Int J Hematol* 81: 307–309.
43. Rajappa S, Uppin SG, Raghunadharao D, Rao IS, Surath A (2004) Isolated central nervous system blast crisis in chronic myeloid leukemia. *Hematol Oncol* 22: 179–181.
44. Bujassoum S, Rifkind J, Lipton JH (2004) Isolated central nervous system relapse in lymphoid blast crisis chronic myeloid leukemia and acute lymphoblastic leukemia in patients on imatinib therapy. *Leuk Lymphoma* 45: 401–403.
45. Porkka K, Koskenvesa P, Lundan T, Rimpilainen J, Mustjoki S, et al. (2008) Dasatinib crosses the blood-brain barrier and is an efficient therapy for central nervous system Philadelphia chromosome-positive leukemia. *Blood* 112: 1005–1012.
46. Ito Y, Pandey P, Mishra N, Kumar S, Narula N, et al. (2001) Targeting of the c-Abl tyrosine kinase to mitochondria in endoplasmic reticulum stress-induced apoptosis. *Mol Cell Biol* 21: 6233–6242.
47. Gonfloni S (2010) DNA damage stress response in germ cells: role of c-Abl and clinical implications. *Oncogene* 29: 6193–6202.
48. Kanning KC, Kaplan A, Henderson CE (2010) Motor neuron diversity in development and disease. *Annu Rev Neurosci* 33: 409–440.
49. Vila M, Przedborski S (2003) Targeting programmed cell death in neurodegenerative diseases. *Nat Rev Neurosci* 4: 365–375.
50. Ludolph AC, Bendotti C, Blaugrund E, Hengerer B, Löffler JP, et al. (2007) Guidelines for the preclinical in vivo evaluation of pharmacological active drugs for ALS/MND: report on the 142nd ENMC international workshop. *Amyotroph Lateral Scler* 8: 217–223.
51. Inoue H, Tsukita K, Iwasato T, Suzuki Y, Tomioka M, et al. (2003) The crucial role of caspase-9 in the disease progression of a transgenic ALS mouse model. *EMBO J* 22: 6665–6674.
52. Campeau E, Ruhl VE, Rodier F, Smith CL, Rahmberg BL, et al. (2009) A versatile viral system for expression and depletion of proteins in mammalian cells. *PLoS One* 4: e6529.
53. Gurney ME, Pu H, Chiu AY, Dal Canto MC, Polchow CY, et al. (1994) Motor neuron degeneration in mice that express a human Cu,Zn superoxide dismutase mutation. *Science* 264: 1772–1775.
54. Adachi H, Kume A, Li M, Nakagomi Y, Niwa H, et al. (2001) Transgenic mice with an expanded CAG repeat controlled by the human AR promoter show polyglutamine nuclear inclusions and neuronal dysfunction without neuronal cell death. *Hum Mol Genet* 10: 1039–1048.

55. Adachi H, Waza M, Tokui K, Katsuno M, Minamiyama M, et al. (2007) CHIP overexpression reduces mutant androgen receptor protein and ameliorates phenotypes of the spinal and bulbar muscular atrophy transgenic mouse model. *J Neurosci* 27: 5115–5126.
56. Minamiyama M, Katsuno M, Adachi H, Waza M, Sang C, et al. (2004) Sodium butyrate ameliorates phenotypic expression in a transgenic mouse model of spinal and bulbar muscular atrophy. *Hum Mol Genet* 13: 1183–1192.
57. Katsuno M, Adachi H, Kume A, Li M, Nakagomi Y, et al. (2002) Testosterone reduction prevents phenotypic expression in a transgenic mouse model of spinal and bulbar muscular atrophy. *Neuron* 35: 843–854.
58. Ishigaki S, Liang Y, Yamamoto M, Niwa J, Ando Y, et al. (2002) X-Linked inhibitor of apoptosis protein is involved in mutant SOD1-mediated neuronal degeneration. *J Neurochem* 82: 576–584.

CROSS-SECTIONAL AND LONGITUDINAL ANALYSIS OF AN OXIDATIVE STRESS BIOMARKER FOR SPINAL AND BULBAR MUSCULAR ATROPHY

TOMOO MANO, MD,¹ MASAHISA KATSUNO, MD, PhD,¹ HARUHIKO BANNO, MD, PhD,^{1,2} KEISUKE SUZUKI, MD, PhD,¹ NORIAKI SUGA, MD,¹ ATSUSHI HASHIZUME, MD, PhD,¹ FUMIAKI TANAKA, MD, PhD,¹ and GEN SOBUE, MD, PhD¹

¹ Department of Neurology, Nagoya University Graduate School of Medicine, 65 Tsurumai-cho, Showa-ku, Nagoya 466-8550, Japan

² Institute for Advanced Research, Nagoya University, Nagoya, Japan

Accepted 6 April 2012

ABSTRACT: *Introduction:* Spinal and bulbar muscular atrophy (SBMA) is an adult-onset motor neuron disease caused by a CAG repeat expansion in the androgen receptor gene. The aim of this study was to verify whether urinary 8-hydroxydeoxyguanosine (8-OHdG), an oxidative stress marker, is a biomarker for SBMA. *Methods:* We measured the levels of urinary 8-OHdG in 33 genetically confirmed SBMA patients and 32 age-matched controls over a 24-month period at 6-month intervals. *Results:* Urinary 8-OHdG levels in SBMA patients were significantly elevated compared with those of controls and correlated well with motor function scores. During the follow-up period, urinary 8-OHdG levels increased and correlated with motor function at each time-point. In addition, urinary 8-OHdG levels at baseline were correlated with changes in the 6-minute walk test during 24 months. *Conclusions:* Urinary 8-OHdG is a biomarker for SBMA, reflecting the severity and possibly predicting the deterioration of motor function.

Muscle Nerve 46: 692–697, 2012

Spinal and bulbar muscular atrophy (SBMA) is an hereditary, adult-onset, lower motor neuron disease. It is caused by aberrant elongation of a trinucleotide CAG repeat, which encodes a polyglutamine tract in the first exon of the androgen receptor (AR) gene.^{1–3} The main symptoms are slowly progressive muscle weakness and atrophy of the bulbar, facial, and limb muscles. In general, the interval between the onset of weakness and death is 10–20 years.⁴ An expanded CAG repeat has been identified as the cause of several neurodegenerative disorders, including SBMA, Huntington disease (HD), and several forms of spinocerebellar ataxia.⁵ Although the causative genes show little homology other than the presence of a CAG repeat, these polyglutamine-mediated disorders share common pathways of molecular pathogenesis, such as transcriptional dysregulation, axonal transport defects, and mitochondrial dysfunction.^{6,7}

Although animal studies have indicated the beneficial effects of androgen deprivation for

SBMA, the results of clinical trials were inconclusive.^{8–10} This is likely attributable to the difficulties in evaluating the disease-modifying effects of the tested drugs due to the slow progression of the neurological symptoms in SBMA. Therefore, appropriate surrogate endpoints are needed to facilitate the proof-of-concept of potential therapies for this disease. In this regard, it is important to identify biomarkers for SBMA that reflect the pathogenic processes and can be used as indicators of therapeutic efficacy. Although the nuclear accumulation of mutant AR protein in the scrotal skin has been shown to be a candidate histopathological biomarker, its practical use is limited due to the invasive nature of the procedure.^{11,12} Conversely, non-invasive serum or urinary markers to evaluate disease severity have not been established for SBMA.

Oxidative stress resulting from mitochondrial dysfunction has been implicated in aging and neurodegeneration.¹³ Pathogenic huntingtin, the causative protein of HD, induces oxidative stress through its direct association with mitochondria and downregulation of mitochondrial transcriptional regulators.^{14,15} In a cellular model of SBMA, the expression of pathogenic AR is associated with depolarization of the mitochondrial membrane and an increase in the levels of reactive oxygen species (ROS), which is attenuated by the antioxidants coenzyme Q10 and idebenone.¹⁶ ROS, such as hydroxyl radicals and H₂O₂, react with guanine residues in DNA and produce 8-hydroxydeoxyguanosine (8-OHdG), which is excreted in the urine, thereby serving as a biomarker of oxidative DNA damage.¹⁷

The aim of this study was to evaluate the validity of urinary 8-OHdG as a biomarker for SBMA. In particular, we investigated whether the urinary levels of 8-OHdG reflect the disease severity of SBMA patients. We also investigated the natural history of this parameter in order to determine whether it can be used to monitor disease progression.

METHODS

Participants. We studied 33 patients with SBMA and 32 age-matched, normal controls (Table 1). The inclusion criteria were: a clinical diagnosis of

Abbreviations: 6MWT, 6-minute walk test; 8-OHdG, 8-hydroxydeoxyguanosine; ALS, amyotrophic lateral sclerosis; ALSFRS-R, ALS Functional Rating Scale-revised; AR, androgen receptor; BMI, body mass index; HbA_{1c}, glycated hemoglobin; HD, Huntington disease; LNS, limb Norris score; NBS, Norris bulbar score; PCR, polymerase chain reaction; ROS, reactive oxygen species; SBMA, spinal and bulbar muscular atrophy

Key words: androgen receptor, biomarker, motor neuron, oxidative stress, spinal and bulbar muscular atrophy

Correspondence to: M. Katsuno; e-mail: ka2no@med.nagoya-u.ac.jp or G. Sobue; e-mail: sobue@med.nagoya-u.ac.jp

© 2012 Wiley Periodicals, Inc.
Published online 31 August 2012 in Wiley Online Library (wileyonlinelibrary.com). DOI 10.1002/mus.23413

Table 1. Clinical and genetic features of the SBMA patients and controls.

Clinical and genetic features	SBMA	Control	P-value
Number of subjects	33	32	
Age at examination (years)	54.7 ± 10.1 (27–72)	52.8 ± 12.8 (36–74)	0.879
BMI*	22.8 ± 3.4 (15.1–27.6)	25.0 ± 6.7 (17.9–29.0)	0.465
CAG repeat length in AR gene	48.4 ± 3.9 (40–57)		
Duration from onset (years)	10.0 ± 6.8 (2–22)		
Hypertension	11 (34.4%)	12 (36.4%)	0.099
Hyperlipidemia	5 (15.6%)	7 (21.2%)	0.299
Diabetes	2 (6.3%)	3 (9.1%)	0.509
HbA _{1c} (%)	5.3 ± 0.5 (4.3–7.2)	5.3 ± 0.4 (4.8–6.1)	0.953

Data are shown as number, mean ± SD (range), or number (%). BMI, body mass index; AR, androgen receptor; HbA_{1c}, glycated hemoglobin.

SBMA with more than 1 motor symptom (i.e., muscle weakness, muscle atrophy, bulbar palsy, and hand tremor) and confirmation by genetic analysis; age between 25 and 75 years; and the ability to walk with or without a cane. We evaluated disease severity using the clinical scales for amyotrophic lateral sclerosis (ALS), such as the limb Norris score (LNS), the Norris bulbar score (NBS), and the ALS Functional Rating Scale-revised; (ALSFRS-R) score. We also measured motor function using clinical tests such as the 6-minute walk test (6MWT) and grip power.^{18,19} We defined the onset of disease as the time when muscle weakness began, but not when tremor of the fingers appeared. The first examination was performed between June and November 2008. All patients were outpatients. In this longitudinal study, the SBMA patients were followed for 24 months at 6-month intervals. During follow-up, 3 patients did not complete the assessment due to difficulty in visiting the hospital regularly. This study conformed to the ethics guidelines for human genome/gene analysis research and epidemiological studies endorsed by the Japanese government. The institutional review board of the Nagoya University Graduate School of Medicine approved the study, and all SBMA patients and normal subjects gave informed consent for participation in the investigation.

Urinary 8-OHdG. Urine samples were obtained from each individual in the morning (9:00 a.m. to 12:00 noon) and were immediately stored at –20°C. Age-matched controls were selected from male examinees undergoing health check-ups between March and April 2009, at the Chuo Clinic, Nagoya. We included control subjects with ages between 25 and 75 years, and those who had any neurological symptoms or findings were excluded. We instructed the patients and controls to avoid strenuous exercise in the 24 h before providing the sample, because it was shown that exercise increases the urinary levels of 8-OHdG.^{20,21} All samples from the same time-point were measured simultaneously. We de-identified the samples, and

the urinary levels of 8-OHdG and creatinine were anonymously measured using an enzyme-linked immunosorbent assay (ELISA) with a specific monoclonal antibody (N45.1; Japan Institute for the Control of Aging, Furoi, Japan) at Mitsubishi Chemical Medicine Co. (Tokyo, Japan).²² The urinary levels of 8-OHdG were normalized in relation to creatinine levels to adjust for the urine volume.

Genetic Analysis. Genomic DNA was extracted from the peripheral blood of SBMA patients using conventional techniques. Polymerase chain reaction (PCR) amplification of the CAG repeat in the AR gene was performed using a fluorescein-labeled forward primer (5'-TCCAGAATCTGTTCCAGAGCG TGC-3') and an unlabeled reverse primer (5'-TGG CCTCGCTCAGGATGTCTTTAAG-3'). The detailed PCR conditions and measurement of the CAG-repeat size have been described elsewhere.²³

Data Analysis. All data are presented as mean ± SD. Patient–control differences in categorical variables were assessed using the chi-square test. Longitudinal changes in the parameters were compared using a paired *t*-test, where the null hypothesis was that there was no change between baseline and the end of the 24-month follow-up. Correlations among the parameters were analyzed using Pearson correlation coefficients. We used multiple regression analysis for multiple classification analysis. *P* < 0.05 and correlation coefficients (*r*) > 0.4 were considered significant. Calculations were performed using SPSS version 14.0J (SPSS Japan, Tokyo, Japan) statistical software.

RESULTS

Clinical Backgrounds and Urinary 8-OHdG Levels in the SBMA Patients. The clinical characteristics of the study population are listed in Table 1. There were a total of 33 SBMA patients in the study. All participants were male and of Japanese nationality. There was no substantial difference between the median CAG repeat length in the SBMA population enrolled in this study and those reported previously.^{4,9,24} Two of the 33 patients needed a cane